Petrology and Chemistry of the Joe Lott Tuff Member of the Mount Belknap Volcanics, Marysvale Volcanic Field, West-Central Utah

U.S. GEOLOGICAL SURVEY PROFESSIONAL PAPER 1354

Petrology and Chemistry of the Joe Lott Tuff Member of the Mount Belknap Volcanics, Marysvale Volcanic Field, West-Central Utah

By KARIN E. BUDDING, CHARLES G. CUNNINGHAM, ROBERT A. ZIELINSKI, THOMAS A. STEVEN, *and* CHARLES R. STERN

U.S. GEOLOGICAL SURVEY PROFESSIONAL PAPER 1354

UNITED STATES GOVERNMENT PRINTING OFFICE, WASHINGTON : 1987

DEPARTMENT OF THE INTERIOR

DONALD PAUL HODEL, *Secretary*

U.S. GEOLOGICAL SURVEY

Dallas L. Peck, *Director*

Library of Congress Cataloging in Publication Data
Petrology and chemistry of the Joe Lott Tuff Member of the Mount Belknap Volcanics, Marysvale volcanic field, west-central Utah.

(Geological Survey professional paper ; 1354)
Bibliography: p.
Supt. of Docs. no.: I 19.16:1354
1. Volcanic ash, tuff, etc.—Utah—Marysvale region. I. Budding, Karin E. II. Series: Geological Survey professional paper ; 1354
QE461.P473 1987 552'.23 86-600023

For sale by the
Books and Open-File Reports Section
U.S. Geological Survey
Federal Center
Box 25425
Denver, CO 80225

PREFACE

Joseph Augustus Lott, born March 10, 1855, was one of nine children of John Smiley Lott and his two wives, Mary Ann Faucett and Docia Emmerine Molen. John Lott was a soldier and settler for the Mormon Church. The Lott cabin, built by John in the mid-1870's, is located in Clear Creek Canyon just east of the mouth of Mill Creek and is typical of pioneer dwellings during Utah's territorial period. The homestead is significant because of its location on the Old Spanish Trail, which was a major trade route in Utah. The cabin was surrounded by cottonwoods and a variety of fruit trees. The Lott's economic survival depended on the production of grains, vegetables, fruit, and stock for home consumption.

Joseph Lott married Marua Twitchell on May 18, 1878, and had four daughters and six sons. They settled in Clear Creek Canyon and farmed. In addition, Joe drove a wagon train up to the miners at the gold and silver mines at Kimberly, 7½ mi south-southwest of the Lott homestead, delivering mail and supplies. The trail and the adjacent creek were named after Joe Lott, and eventually the rocks forming the canyon walls of Joe Lott Creek and lower Clear Creek became formally named the Joe Lott Tuff Member of the Mount Belknap Volcanics. (Historical information courtesy of the Utah Genealogical Society, Salt Lake City, Utah.)

By KARIN E. BUDDING, CHARLES G. CUNNINGHAM, ROBERT A. ZIELINSKI, THOMAS A. STEVEN, *and* CHARLES R. STERN

CONTENTS

ILLUSTRATIONS

TABLES

PETROLOGY AND CHEMISTRY OF THE JOE LOTT TUFF MEMBER OF THE MOUNT BELKNAP VOLCANICS, MARYSVALE VOLCANIC FIELD, WEST-CENTRAL UTAH

By KARIN E. BUDDING, CHARLES G. CUNNINGHAM, ROBERT A. ZIELINSKI, THOMAS A. STEVEN, and CHARLES R. STERN

ABSTRACT

The Joe Lott Tuff Member of the Mount Belknap Volcanics is the largest (150 km^3) rhyolitic ash-flow tuff sheet in the Marysvale volcanic field. It was erupted about 19 Ma, shortly after the changeover from intermediate-composition calc-alkaline volcanism to bimodal basalt-rhyolite volcanism. Eruption of the tuff resulted in the collapse of the Mount Belknap caldera, and the pyroclastic intracaldera stratigraphy parallels that observed in the outflow facies. The Joe Lott Tuff Member is a composite ash-flow tuff sheet that changes laterally from a simple cooling unit near its source to four distinct cooling units toward its distal end. The lowest of these units is the largest and most widespread; where it is best exposed in Clear Creek Canyon, it is as much as 64 m thick and has a basal vitrophyre. Eruption of the lower unit led to the initial collapse of the caldera. Along Clear Creek, the lower unit is followed upward in stratigraphic succession by a middle unit as much as 43 m thick, a pink-colored unit 26 m thick containing a prominent air-fall layer within it, and an upper unit 31 m thick.

The Joe Lott Tuff Member is an alkali rhyolite with 75.9–77.3 wt percent silica and 8.06–9.32 wt percent $K_2O + Na_2O$; the agpaitic index [molar $(Na_2O + K_2O)/Al_2O_3$] is 0.77–0.98. Most of the tuff contains about 1 percent phenocrysts of quartz, sanidine, biotite, oxidized Fe-Ti oxides, augite, oligoclase, apatite, zircon, and sphene. The basal vitrophyre contains accessory allanite and chevkinite.

The geochemical history of the Joe Lott Tuff Member is difficult to interpret because of its age, the general lack of glassy samples, and the narrow range of abundance of key chemical elements. Compositional discontinuities within the lower cooling unit and between the different cooling units of the Joe Lott Tuff Member are best documented by (1) the composition and relative proportion of sanidine and (2) whole-rock abundances of SiO_2, K_2O, CaO, and certain trace elements that are relatively resistant to postmagmatic redistribution (REE, Sc, Co, Cr, Y). The compositional discontinuities suggest chemical perturbations of the magma during and between eruptions of cooling units. Vertical gradients in temperature and volatile content within the pre-eruptive magma chamber are indicated by roofward decrease in phenocryst content and increase in hydrous silicates, as recorded in the lower cooling unit. Normative compositions of the phenocryst-poor rhyolites plot near the ternary minimum in the Or-Ab-Q system at $P_{H_2O}=1$ kb and indicate pre-eruptive temperatures near 750°C.

The chemical homogeneity of phenocrysts at a given stratigraphic level, the distribution of relatively large or dense phenocrysts, and the trace-element chemistry of the lower cooling unit are not compatible with a model of evolution by open-system fractional crystallization in the pre-eruptive magma chamber. Chemical gradients in the basal vitrophyre of the lower cooling unit show 150 to 600 percent enrichments of Cs, U, Mo, Co, and Cr. Such great enrichments are not compatible with the small degree of crystallization that is indicated by phenocryst contents of <1 to 3 modal percent. Furthermore, Cs, U, and Mo are subject to redistribution during postmagmatic devitrification, hydration, and alteration, and these processes could have created the apparent enrichments in the basal vitrophyre. In addition, enrichments of Co and Cr in the basal vitrophyre may be slightly influenced by minor incorporation of more mafic lithic fragments from underlying rocks. Therefore, the chemical signature of the basal vitrophyre may be the result of both magmatic and postmagmatic processes. REE, Sc, Y, and Co and Cr are considered relatively resistant to postmagmatic redistribution; the distribution of these elements in the lower cooling unit indicates a much smaller roofward enrichment in the magma chamber—only 5 to 15 percent. If only these latter compositional variations are considered magmatic, the data are insufficient to support a model of liquid-state differentiation (thermogravitational diffusion). An alternative model calls for limited fractional crystallization and crystal-melt separation *at depth*, near contacts between magma and wall rock.

INTRODUCTION

Large-volume silicic magma chambers are zoned chemically and thermally, and voluminous ash-flow tuff sheets provide quenched samples of such chambers, arranged in an inverted stratigraphic order. Compositions of these rocks reflect the vertical gradients in physical and chemical properties of the magmas immediately prior to eruption and allow modeling of the processes of fractionation that caused the zonation. With increasing depth in a chamber, the phenocryst content and temperature commonly increase as the magma becomes less silicic, as has been documented for the Bandelier Tuff, New Mexico (Smith and Bailey, 1966), and for the Paintbrush Tuff, Nevada (Lipman and others, 1966).

The Mount Belknap caldera in the Marysvale volcanic field of west-central Utah collapsed about 19 Ma with the eruption of 150 km^3 of pyroclastic material collectively termed the Joe Lott Tuff Member of the Mount

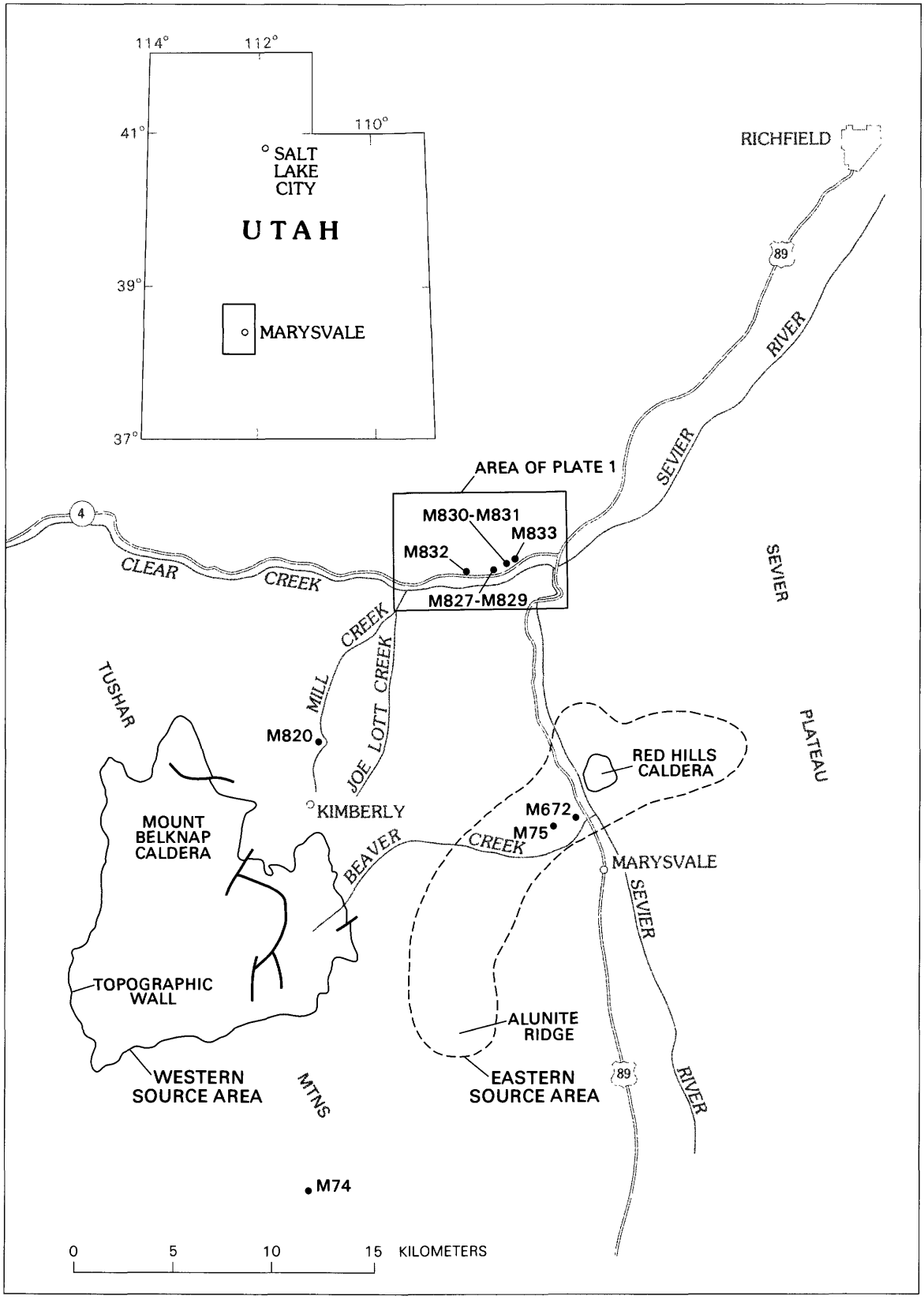

FIGURE 1.—Index map showing the location of the western and eastern source areas of the Mount Belknap Volcanics, the Mount Belknap and Red Hills calderas, the area mapped in detail for this study (pl. 1), sample localities, and principal geographic features mentioned in the text.

Belknap Volcanics. Data presented here from field mapping, petrography, and chemical analysis of whole rocks and phenocrysts define processes taking place within the source magma chamber and are compared with similar data from younger calderas. This study is part of a larger, ongoing study of the Marysvale volcanic field and associated ore deposits (Steven and others, 1981; Budding, 1982; Cunningham, Steven, Rowley, and others, 1983, 1984; Steven and Morris, 1983; Cunningham, Rye, and others, 1984; Steven, Rowley, and Cunningham, 1984).

ACKNOWLEDGMENTS

We thank Ralph P. Christian, Eugene E. Foord, Lori B. Glassgold, Harald H. Mehnert, and Ray E. Wilcox for their assistance with analytical determinations, and Wes Hildreth, Edwin E. Larson, and Gail A. Mahood for perceptive advice and discussions.

GEOLOGIC SETTING

Marysvale, Utah, is located in the north-trending Marysvale Valley 260 km south of Salt Lake City, within the Marysvale volcanic field (fig. 1). The surrounding volcanic field covers more than 2,000 km^2 in west-central Utah and lies largely in the High Plateaus physiographic subprovince in the transition zone between the Colorado Plateau Province to the east and the Basin and Range Province to the west. The Marysvale Valley has an elevation of about 2,000 m and is bordered on the west by the Tushar Mountains (maxiumu altitude 3,700 m) and on the east by the Sevier Plateau (2,900 m).

The volcanic rocks in the Marysvale area lie unconformably on Paleozoic, Mesozoic, and lower Cenozoic sedimentary rocks. Volcanic rocks in the center of the pile are intermediate-composition, calc-alkaline lava flows, volcanic breccia, volcaniclastic deposits, and ash-flow tuffs of the Bullion Canyon Volcanics. These rocks are between 22 and 35 Ma and originally formed scattered and partially clustered stratovolcanoes. Quartz monzonite stocks intruded vent-facies rocks in the cores and flanks of some of these intermediate-composition volcanoes about 23 Ma near the end of calc-alkaline volcanic activity. Local thicknesses of the Bullion Canyon Volcanics range from 100 to 200 m at the eroded edges of the pile to more than 1 km near the center of the area (Steven and others, 1979).

The composition of the volcanic rocks changed abruptly to a bimodal baslt-rhyolite assemblage about 21 Ma at the beginning of extensional basin and range tectonism in adjacent parts of the Great Basin. Silicic alkali rhyolite lava domes, lava flows, and ash-flow tuffs were extruded from a western source area at the Mount Belknap caldera, 20 km west of Marysvale, and from an eastern source area extending from about 9 km northeast of Marysvale to about 12 km southwest of Marysvale (fig. 1). The combined volcanic rocks from the two source areas compose the Mount Belknap Volcanics, which at one time covered an area greater than 600 km^2. Most of the Mount Belknap Volcanics was derived from the western source area where eruption of the Joe Lott Tuff Member resulted in collapse of the Mount Belknap caldera. In the eastern source area, the Red Hills caldera formed shortly thereafter as a result of the eruption of the Red Hills Tuff Member. Both calderas formed about 19 Ma. Igneous activity that produced the upper members of the Mount Belknap Volcanics continued in the western source area until around 16 Ma and in the eastern source area until about 14 Ma (Cunningham, Steven, Campbell, and others, 1984).

The Miocene and Pliocene Sevier River Formation, consisting of fluviatile and minor lacustrine sedimentary rocks, was deposited in basins developed concurrently with basin-and-range extension. Many local ash-fall tuffs within the Sevier River Formation indicate that episodic volcanic activity occurred in the area during this period of sedimentation. Widely erupted but small-volume tholeiitic basalt lava flows are locally interleaved with the Sevier River sedimentary rocks (Steven and others, 1979; Best and others, 1980). A 5.4-Ma rhyolite dome, erupted in a canyon cut in the Sevier Plateau, indicates that the present distribution of plateaus and basins had been developed by late Miocene time (Rowley and others, 1981).

MOUNT BELKNAP CALDERA

As described by Cunningham and Steven (1979) and Steven, Rowley, and Cunningham (1984), the Mount Belknap caldera in the central Tushar Mountains (fig. 1) developed in a hilly terrain eroded on clustered Bullion Canyon central-vent volcanoes. Minor premonitory Mount Belknap eruptions probably extruded small rhyolite lava flows in the source area, inasmuch as fragments of these rocks have been found near the base of the outflow ash-flow tuff in areas adjacent to the caldera. This early activity was followed by catastrophic eruption of many tens of cubic kilometers of ash-flow tuff that formed the Joe Lott Tuff Member and led to collapse of the Mount Belknap caldera. Large-volume eruptions continued after subsidence and filled the caldera depression to overflowing with ash-flow tuff and rhyolite lava flows. Some of this intracaldera tuff is continuous across the caldera rim into the upper part of the outflow Joe Lott. The pyroclastic volcanic activity took place within a short time span, within the analytical uncertainty of the age of the tuff, 19.2 ± 0.4 Ma.

TABLE 1.—*Inferred correlation between the sequence of rocks in the intracaldera fill of the Mount Belknap caldera and the outflow section described in this report*

MOUNT BELKNAP CALDERA INTRACALDERA FILL (Intracaldera facies of the Mount Belknap Volcanics)	OUTFLOW SECTION DESCRIBED IN THIS REPORT (Outflow facies of the Mount Belknap Volcanics)	
Intracaldera stocks	Crystal-rich tuff member	
Upper tuff member	Upper unit Pink unit	Joe Lott Tuff Member
Volcanic breccia member		
Mount Baldy Rhyolite Member		
Middle tuff member	Middle unit	
Blue Lake Rhyolite Member		
Lower tuff member	Lower unit	

The irregularly shaped topographic outline of the caldera is 13 km wide east-west and 17 km long north-south (fig. 2). The caldera fill consists of more than 1 km of rhyolite ash-flow tuff, lava flows, lava domes, and volcanic breccia (table 1). The intracaldera ash-flow tuff units are lithologically and compositionally virtually identical with the outflow Joe Lott Tuff Member, and the lava flows have closely similar compositions. The lowest stratigraphic unit exposed within the caldera is the lower tuff member, an alkali rhyolite ash-flow tuff containing less than 1 percent phenocrysts of quartz, sanidine, plagioclase, and biotite in a devitrified groundmass. The lower tuff member is at least 450 m thick, and the base is not exposed. The overlying Blue Lake Rhyolite Member consists of contorted, flow-layered rhyolite lava flows 560 m thick in the southern and western parts of the caldera. It wedges out northward and is absent in the northern part of the caldera. The next highest stratigraphic unit is the middle tuff member, which is also an alkali rhyolite ash-flow tuff compositionally and lithologically indistinguishable from the lower tuff member. It is 500 m thick on the north side of the caldera where it overlaps the topographic wall and is continuous with the upper part of the simple cooling unit that forms the proximal outflow part of the Joe Lott Tuff Member. The middle tuff member wedges out southward against bulbous Blue Lake lava flows and domes. The overlying Mount Baldy Rhyolite Member consists of a series of alkali rhyolite lava flows and domes containing variable amounts of small sanidine phenocrysts. Most of the Mount Baldy domes are located in the southern and northwestern parts of the caldera where they rest directly on similar rocks in the Blue Lake Rhyolite Member. Some of the Mount Baldy domes and flows are flanked by wedges of talus and mud-flow breccia. The stratigraphically highest part of the caldera fill consists of small patches of alkali rhyolite ash-flow tuff that is indistinguishable from the lower and middle tuff members; these remnants are present on the tops of hills in the northwestern part of the caldera. The caldera fill is cut by three known rhyolite stocks: the largest, 1.3 by 0.6 km across, is in the headwaters of the North Fork of North Creek; a highly porphyritic stock less than 100 m across is present at the U-Beva uranium prospect farther downstream; and a small stock only a few tens of meters across with an associated intrusive breccia crops out near the southern end of Gold Mountain. Fragments of intrusive rock and associated molybdenum-bearing quartz veins are on an old mine dump west of Gold Mountain, above the projected structural margin of the caldera. The central core of the Mount Belknap caldera was not resurgently domed during later stages of its cycle of development. Instead, the caldera fill subsided further when a tilted trapdoor block sank an additional 150 m along an arcuate fault believed to overlie the northeastern part of the buried structural margin of the caldera.

The succession within the caldera fill documents that the caldera formed and filled during a series of eruptions that alternated from violent pyroclastic episodes to more quiet effusion of lava. The irregular shape of the topographic wall (fig. 2) probably formed when unsupported caldera walls caved inward during and shortly after collapse. The irregularity developed as weaker parts of the wall broke away more readily than the more cohesive parts. The cyclic nature of eruptions is also reflected in some of the chemical gradients within

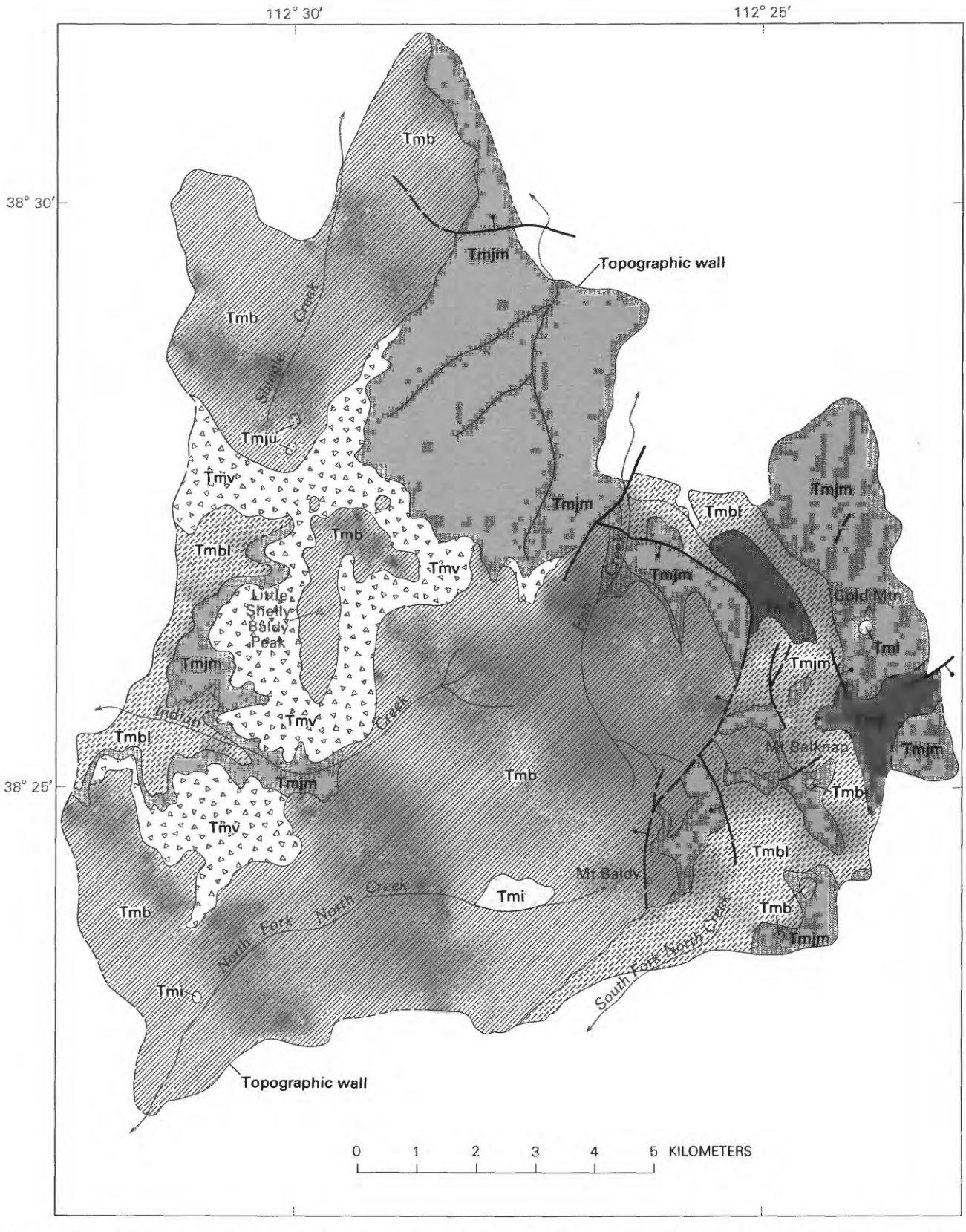

FIGURE 2.—Geologic map of the Mount Belknap caldera (outline dashed where incompletely exposed). All patterned rock units belong to the intracaldera facies of the Mount Belknap Volcanics: Tmjl, lower tuff member; Tmbl, Blue Lake Rhyolite Member; Tmjm, middle tuff member; Tmb, Mount Baldy Rhyolite Member; Tmju, upper tuff member; Tmv, volcanic breccia member; and Tmi, intrusive rock. Heavy lines, faults (dashed where inferred), bar and ball on downdropped side. Modified from Cunningham and Steven (1979).

individual cooling units, as documented under "Compositional Variations in the Joe Lott Tuff Member."

On the basis of the interpreted position of the structural margin, the high-level magma chamber is thought to have been broad (at least 10 km across) with the subsided block being about 9 to 10 km across. Assuming water saturation, a P_{H_2O} of 800 ± 200 bars in the magma is obtained by plotting the average normative mineral compositions (Q-Or-Ab) of the Joe Lott Tuff Member (Cunningham and Steven, 1979) on the projection of the quaternary system Q-Or-Ab-H_2O (Tuttle and Bowen, 1958). This pressure represents an equivalent lithostatic depth of 3 to 4 km, which is thought to be a realistic depth to the top of the magma prior to eruption (Cunningham and Steven, 1979).

A structural model of the Mount Belknap caldera is based on its surface area of 148 km^2, ring-fracture radius of about 4.8 km, and steeply inward-dipping topographic walls. At a 45° dip, the walls meet the structural margin at a depth of about 2 km, containing a cone-shaped volume of about 150 km^3. This intracaldera volume is comparable to the outflow volume of Joe Lott Tuff Member, on the basis of observations of areal extent and average thicknesses.

GEOCHRONOLOGY

Prior to this study, no ages were available for the Joe Lott Tuff Member; however, stratigraphic relationships with dated overlying and underlying rock units indicated an age of approximately 19 Ma. An underlying ash-flow tuff (belonging to the lower heterogeneous member of the Mount Belknap Volcanics) gave fission-track ages of 19.6 ± 0.8 Ma on zircon and 18.8 ± 1.7 Ma on apatite (Steven and others, 1979). The Red Hills Tuff Member, which overlies the Joe Lott Tuff Member, has a K-Ar age on sanidine of 18.9 ± 0.7 Ma (Cunningham, Ludwig, and others, 1982).

Two samples of the Joe Lott Tuff Member—the upper unit (sample no. M833) and the basal vitrophyre (M820)—were dated by the K-Ar method by Harald H. Mehnert and Glen A. Izett of the U.S. Geological Survey. Sanidine from the upper cooling unit gave an age of 18.3 ± 1.1 Ma (table 2), and glass from the basal vitrophyre yielded a whole-rock age of 17.2 ± 0.7 Ma. By comparison with the other ages available, the 17.2 ± 0.7 Ma age of the basal vitrophyre is considered to be too young; the discordance is attributed to a loss of argon related to hydration of the volcanic glass (Dalrymple and Lanphere, 1969). The dull appearance and 2.8 wt percent water of the vitrophyre indicate that it is significantly hydrated. The best age for the Joe Lott Tuff Member, considering the analytical uncertainties of all ages that were determined, is 19.2 ± 0.4 Ma; this interpreted age allows the age of the Joe Lott Tuff Member to be concordant with the ages already determined for earlier- and later-erupted units.

JOE LOTT TUFF MEMBER OF THE MOUNT BELKNAP VOLCANICS

The Joe Lott Tuff Member is the largest ash-flow tuff unit in the Mount Belknap Volcanics, and its eruption was associated with the collapse of the Mount Belknap caldera. It is a high-silica, crystal-poor alkali rhyolite. The member is widely distributed around the caldera, and widespread sheets of the tuff north and south of the caldera overlie fairly flat lying volcaniclastic beds, lava flows, and ash-flow tuffs of the Bullion Canyon Volcanics. Near the source, the Joe Lott is red and dense and forms a simple cooling unit. A lateral transition is evident in color and degree of welding (fig. 3), and in its distal parts, the Joe Lott Tuff Member is gray and forms a composite cooling unit made up of at least four ash-flow tuff cooling units.

The largest outcrop area of the Joe Lott Tuff Member, as well as the best exposures of the multiple cooling units that compose it, flanks Clear Creek Canyon west of U.S. Highway 89 (fig. 1). The exposures along Clear Creek in the southern parts of T. 25 S., Rs. 4 and 4½ W. are designated the principal reference locality. Most of the detailed studies leading to this report were done along Clear Creek (fig. 1) in the area labeled plate 1. In this area, the Joe Lott Tuff Member overlies the Three Creeks Tuff Member of the Bullion Canyon Volcanics and is overlain by somewhat consolidated sands and gravels of the Sevier River Formation. Four cooling units that were delineated in mapping the outflow Joe Lott Tuff Member here consist, from the base upward, of the lower, middle, pink, and upper units (fig. 4).

The most complete and impressive exposure of the lower, middle, and upper cooling units is at the eastern end of Clear Creek Canyon (fig. 5) where clearly defined erosional benches separate the units. The approximate thickness of each cooling unit at this locality is 64 m, lower unit; 43 m, middle unit; and 31 m, upper unit. The pink unit is absent at this locality but is well exposed farther west in Clear Creek Canyon where it is at most about 26 m thick.

The sequence of ash-flow tuff units in the outflow section along Clear Creek correlates well with the sequence within the Mount Belknap caldera (table 1). The lower unit in the outflow sheet was deposited by ash flows from the earliest major pyroclastic eruptions at the source, which probably led to the main collapse of the Mount Belknap caldera; we assume that it corre-

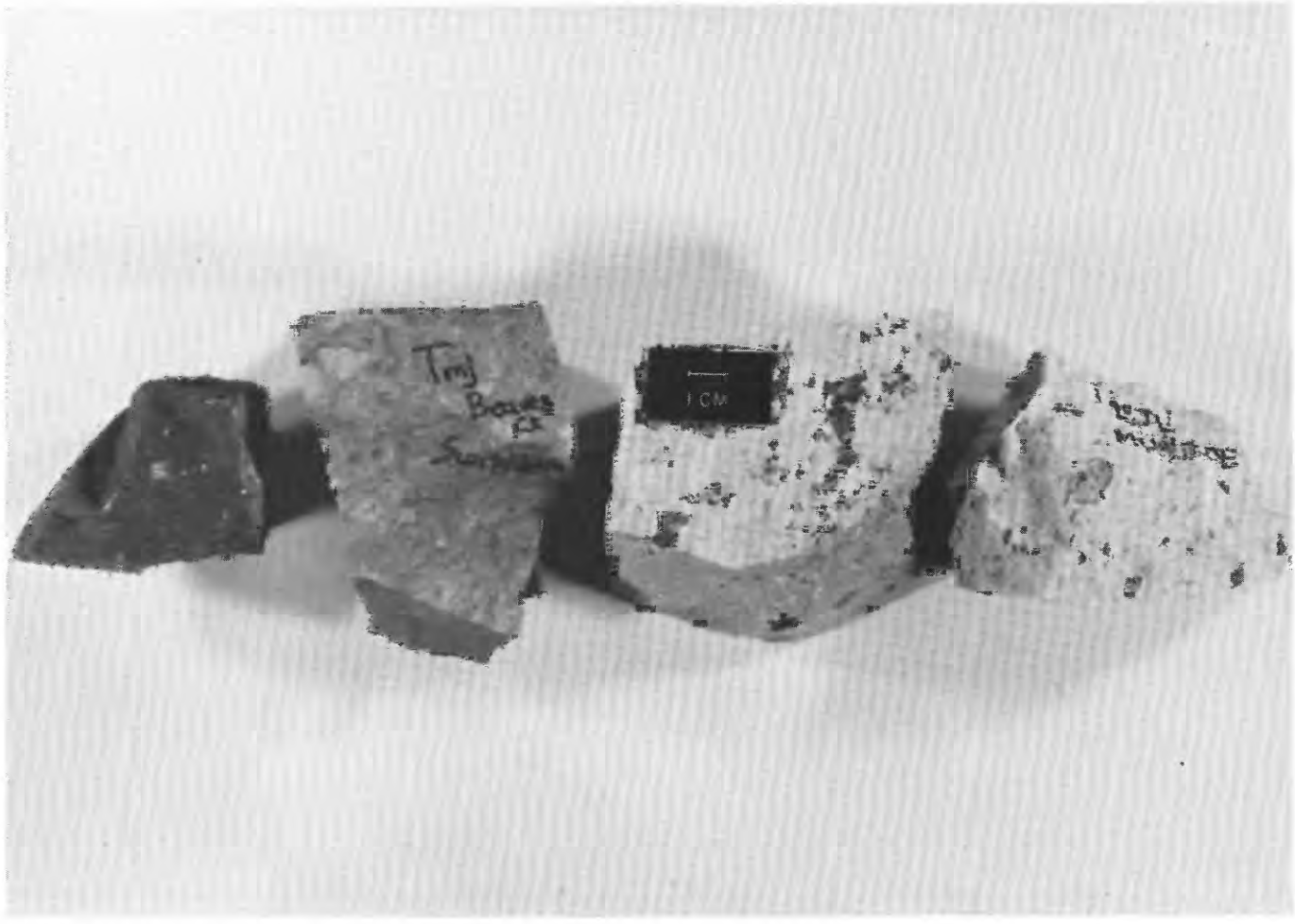

FIGURE 3.—Hand samples illustrating the lateral transition of the Joe Lott Tuff Member from red, dense rock near the source (on the left) to gray, poorly welded rock in the distal parts of the ash-flow sheet (on the right). All samples shown are devitrified and change in degree of welding from densely welded on the left to poorly welded with vapor-phase crystallization on the right.

lates with the lower tuff member of the intracaldera facies which is the oldest unit known to have been deposited within the caldera. The cooling break at the top of the lower outflow unit marks a time without significant pyroclastic eruptions, perhaps being represented within the caldera by accumulation of the rhyolite lava flows and domes of the Blue Lake Rhyolite Member. The thick middle unit in the outflow sheet in Clear Creek Canyon chronicles renewed major ash-flow eruptions at the source and probably is equivalent to the middle tuff member of the intracaldera facies; this probability is supported by the physical continuity across the rim of the caldera of the middle tuff member of the intracaldera facies with the upper part of the simple cooling unit of outflow Joe Lott adjacent to the caldera. This simple cooling unit seems to be equivalent largely to the lower and middle units in the Clear Creek Canyon section. The complete cooling break at the top of the middle unit in Clear Creek Canyon again represents a time of minimal pyroclastic eruptions, which probably was represented within the caldera by extrusion of the Mount Baldy Rhyolite Member. By the logic of these parallel successions, the upper tuff member within the caldera probably is equivalent to either the pink unit or the overlying upper unit in the Clear Creek Canyon section.

The Joe Lott Tuff Member is thickest in two paleovalleys that radiate from the Mount Belknap caldera. One paleovalley was along the present location of Mill Creek (fig. 1), and the ash flows that came down that valley continued northward to form the section that was studied in detail at the east end of Clear Creek. The other paleovalley was along the present location of Beaver Creek (fig. 1) and trended eastward toward Marysvale. In the upper parts of these paleovalleys, the Joe Lott Tuff Member consists of a simple cooling unit that appears to have been made up mostly of the lower and middle distal cooling units, but the

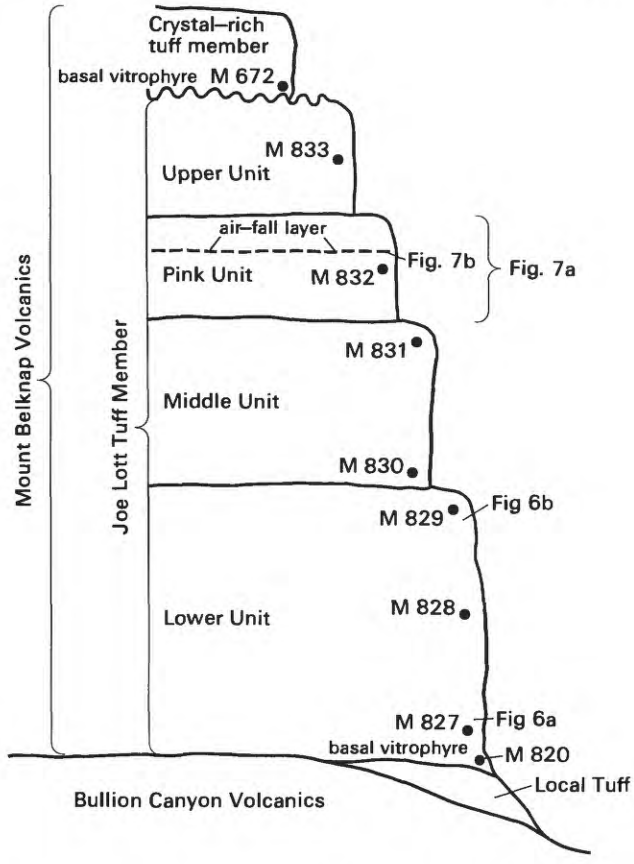

FIGURE 4.—Diagrammatic sketch of stratigraphic relationship of the Bullion Canyon Volcanics, the lower, middle, pink, and upper units of the Joe Lott Tuff Member, and the crystal-rich tuff member of the Mount Belknap Volcanics. Includes sample and photograph locations.

location of the contact between them cannot be distinguished. The tuff in the simple cooling unit is a pink, moderately densely welded, massive, and megascopically homogeneous rock in which former pumice fragments are obscured. The rock typically weathers into small plates that resemble wood chips around a chopping block. A basal vitrophyre is exposed in only one locality, approximately 8 km south of Clear Creek, along Mill Creek (fig. 1), where it consists of a black glass containing a moderate amount of small, flow-banded, rhyolite, lithic fragments. The bottom of the cooling unit exposed along Beaver Creek is devitrified to the base, which rests upon the eroded Bullion Canyon Volcanics. Locally, rhyolite lava flows and small ash-flow tuffs are present beneath the cooling unit.

The lower cooling unit in the composite section along Clear Creek is the most widespread of the distal units. The base of the lower cooling unit in the Clear Creek section is densely welded, purplish-gray rock and contains rhyolite lithic fragments. Cognate pumice fragments are flattened in the plane of compaction foliation to form fiamme (fig. 6). Fracturing parallel to the foliation has resulted in horizontal platy jointing near the base of the unit. The overlying moderately welded part of the unit is completely devitrified, massive, and characterized by columnar jointing from tensional cooling. The upper part is moderately welded, devitrified, and contains pumice fragments that are devitrified but only slightly compacted. The unit grades upward into a poorly welded, purplish-white, somewhat chalky rock at the top.

The middle cooling unit is virtually identical to the lower cooling unit in the Clear Creek section where it consists of a massive, light-gray, moderately welded, columnar-jointed rock. A 1-m-thick, pink to light-purple, pumice-rich, crossbedded ground surge deposit is locally present at the bottom of the middle cooling unit. Near the base, the middle unit is a moderately welded gray rock with as much as 5 percent rhyolite lithic fragments and 2 percent Bullion Canyon Volcanics lithic fragments. Near the top of this unit, the rock becomes poorly welded and lighter in color.

The pink cooling unit, which lies between the middle and upper units, is a poorly welded, pumice-rich, easily erodable rock that has a prominent, pervasive pink color. It consists of two ash-flow tuffs (fig. 7a) separated by a prominent air-fall layer. The pink unit is present in the Clear Creek area where it forms a definite marker that wedges out eastward (pl. 1). At a point 4.2 km west of the intersection of Highways 4 and 89, the ash-flow sheet below the air-fall layer is 17 m thick, the air-fall layer is 0.5 m thick, and the overlying ash-flow sheet is 9 m thick. The pink color of the unit is due to oxidation of iron, and the uniform distribution suggests that the coloration is a primary feature perhaps related to eruption of the unit through a caldera lake.

The air-fall layer within the pink unit consists of three prominent graded layers that are exceptionally uniform over a lateral distance of about 2 km (fig. 7b). The fragments include pieces of rhyolite, pumice, and obsidian. The laminar layers show no signs of crossbedding, scouring, slump features, or other indications of being reworked by water.

The upper cooling unit is similar in appearance to the upper part of the lower cooling unit; it is a light-gray, devitrified, moderately to poorly welded, massive rock, containing slightly compacted pumice fragments. It contains less than 1 percent phenocrysts, mostly of sanidine, quartz, oligoclase, biotite, apatite, zircon, and Fe-Ti oxide minerals and as much as 5 percent rhyolitic lithic fragments 2 cm or less in diameter near the base.

FIGURE 5.—Joe Lott Tuff Member composite ash-flow tuff sheet, along the eastern end of Clear Creek Canyon, showing the most complete section where the lower, middle, and upper units were measured and sampled.

TABLE 2.—*Data for K-Ar ages of the Joe Lott Tuff Member*

Sample No.	Lab No.	Material	K_2O %	$^{40}Ar^*$ (10^{-10} mol/g)	% radiogenic argon	Age in Ma ±2σ
M833	DKA4127	Sanidine	5.56, 5.68[1]	1.487	61.3	18.3±1.1
M820	DKA4126	Vitrophyre	4.83, 4.85[1]	1.204	68.6	17.2±0.7

[1]Determined by flame photometry.

Decay constants for ^{40}K

$\lambda_\varepsilon e^+ e\xi = 0.581 \times 10^{-10}$/yr

$\lambda_\beta = 4.962 \times 10^{-10}$/yr

$^{40}K/K = 1.167 \times 10^{-4}$ atom %

FIGURE 6.—Densely welded base of the lower cooling unit of the Joe Lott Tuff Member showing pumice fragments flattened in plane of compaction foliation to form fiamme.

CRYSTAL-RICH TUFF MEMBER OF THE MOUNT BELKNAP VOLCANICS

The crystal-rich tuff member was erupted from the Mount Belknap caldera source area 19.0±1.2 Ma (Steven and others, 1979). It is the only major outflow ash-flow tuff unit from this source other than the Joe Lott Tuff Member, which the crystal-rich tuff member unconformably overlies. Most of the member forms a major cooling unit, about 15 m thick, which is overlain by one or two relatively thin cooling units of similar lithology. Each cooling unit has a basal vitrophyre. South and east of the caldera, the crystal-rich tuff member fills paleochannels that radiate outward from the caldera. The cross section of one of these channels is well exposed along Beaver Creek (fig. 1), 4.5 km west of U.S. Highway 89. The crystal-rich member consists of moderately welded alkali rhyolite ash-flow tuff containing 22 percent phenocrysts of quartz, alkali feldspar, plagioclase, biotite, augite, apatite, zircon, and Fe-Ti oxide minerals. It also contains about 3 percent rhyolite lithic fragments.

SAMPLE LOCATIONS AND DESCRIPTIONS

A suite of nine samples, each about 50 kg in size, was collected from the Joe Lott Tuff Member and the crystal-rich tuff member to describe the chemistry and mineralogy of rocks derived from the Mount Belknap caldera source area. Owing to the low phenocryst content, high degree of welding, and possible secondary chemical modifications by ground water, it was not feasible to restrict sample collection to pumice; instead the freshest available whole rock was collected at each site. Four samples, including one from the basal vitrophyre, were collected from the relatively thick lower cooling unit. Two samples were taken from the thinner

TABLE 3.—*Locations of analyzed samples from the Joe Lott Tuff Member and the crystal-rich tuff member*

Sample No.	Description	Location (see fig. 1)
M672	Crystal-rich tuff member, vitrophyre	3.2 km north of Marysvale on U.S. Highway 89
	Joe Lott Tuff Member	
M833	Upper unit	2.0 km west of U.S. Highway 89 on State Road 4
M832	Pink unit	4.2 km west of U.S. Highway 89 on State Road 4
M831	Middle unit--top	2.1 km west of U.S. Highway 89 on State Road 4
M830	Middle unit--bottom	
M829	Lower unit--top	2.9 km west of U.S. Highway 89 on State Road 4
M828	Lower unit--middle	
M827	Lower unit--bottom	
M820	Lower unit--vitrophyre	8 km south of State Road 4 along Mill Creek

middle cooling unit and one sample each from the pink and upper cooling units and from the crystal-rich tuff member.

Locations and modal analyses for each of the samples are given in tables 3 and 4. The modal analyses are based on 1,000 points counted exclusive of lithic fragments. Because of the low phenocryst content (about 1 percent) of the Joe Lott Tuff Member, the modal abundances of mineral phases are subject to large errors; therefore, for the thin-section data, only the presence or absence of the mineral is reported. The paucity of crystals in the Joe Lott Tuff Member indicates that the magma was erupted when very near its liquidus.

With the exception of the vitrophyre, all samples of the Joe Lott Tuff Member have devitrified groundmasses. Spherulitic devitrification textures are common in the pumice fragments, and former glass shards commonly exhibit axiolitic textures. Rhyolite lithic fragments are common but of generally low abundance. Vapor-phase crystallization of quartz, cryptocrystalline silica, and feldspar has occurred in lithophysal cavities. Compaction of the glass shards varies greatly.

The major differences observed among samples of the Joe Lott Tuff Member are variations in degree of welding and abundance of phenocryst phases. By far the most densely welded rocks are at the base of the lower cooling unit (fig. 8). Welding decreases upward in both the lower and middle cooling units; this condition reflects lower temperatures at the time of accumulation, less compaction within the thinner overlying sheets, or both.

The upward increase of quartz, total feldspar, and the plagioclase to sanidine ratio in the lower cooling unit reflects an increase in crystal content with depth in the magma chamber, a common feature of zoned silicic magma chambers (Lipman and others, 1966; Smith, 1979). The same crystal content gradient is present in the middle unit. These relations suggest either restratification of the magma chamber between periods of eruption or, less likely, renewed tapping of a chemical gradient incompletely erupted and not vertically disturbed during the first eruption period.

WHOLE-ROCK CHEMISTRY

Major-element compositions and CIPW norms of whole-rock samples are listed in table 5. The major elements were analyzed by X-ray fluorescence or by a combination of atomic absorption and colorimetric methods (rapid-rock analysis: Shapiro, 1975). Loss on ignition (LOI), H_2O^+, and H_2O^- were determined on

TABLE 4.—*Modal abundances, in percent, and thin-section descriptions of the Joe Lott Tuff Member and the crystal-rich tuff member*

[Presence (+), absence (-); for location of samples see fig. 1]

Sample	Groundmass	Total phenocrysts	Quartz	Sanidine	Plagioclase	Biotite	Augite	Fe-Ti oxides	Apatite + zircon
Crystal-rich tuff member,									
vitrophyre (M672)-------	78.1	21.9	15.2	4.7	0.1[1]	0.7	0.5	0.7	+
Joe Lott Tuff Member									
Upper unit (M833)-------	99.0	1.0	+	+	+	+	+	+	+
Pink unit (M832)--------	99.3	.7	+	+	+	+	+	+	+
Middle unit--top (M831)	99.0	1.0	+	+	+	-	+	+	+
Middle unit--bottom									
(M830)----------	99.6	.4	-	+	+	+	+	+	+
Lower unit--top (M829)-	96.9	3.1	+	+	+	+	+	+	+
Lower unit--middle									
(M828)----------	99.3	.7	+	+	+	+	+	+	+
Lower unit--bottom									
(M827)----------	99.4	.6	-	+	+	+	+	+	+
Lower unit--vitrophyre									
(M820)----------	99.7	.3	+	+	+	+	+	+	+

Sample	*Description*
Crystal-rich tuff member, vitrophyre	Glassy groundmass with small quantities of pumice fragments. Contains ubiquitous euhedral and subhedral phenocrysts of quartz, some embayed, ranging from 3.6 mm to 0.1 mm. Euhedral and subhedral sanidine, including microlites and some embayed grains, are 0.04 to 3.4 mm. Andesine averages 0.4 mm. Yellowish-brown to dark-brown biotite plates average 0.4 mm, but as much as 2.2 mm in length. Light-green subhedral augite commonly with opaque inclusions averages 0.4 mm. Minor Fe-Ti oxides and other opaque minerals.
Joe Lott Tuff Member	
Upper unit	Poorly welded, devitrified groundmass of glass shards and large spherulitically devitrified pumice fragments. Axiolitic structure on devitrified rims of lithophysal cavities, some with vapor-phase crystals. Minor quartz averages 0.5 mm; sanidine, 0.2 mm; oligoclase, 0.4 mm.
Pink unit	Glassy groundmass consists of densely concentrated, poorly welded, large, broken glass shards. Quartz phenocrysts average 0.5 mm. Elongated tubular pore spaces give fibrous structure to 1.5 mm pumice fragments. Some pumice fragments are devitrified.
Middle unit—top	Poorly welded, devitrified groundmass of shards and pumice. Axiolitic structure on devitrified rims of lithophysal cavities, some with vapor-phase crystals. Some remobilized silica found with devitrification products. Quartz phenocrysts average 0.5 mm; zircon, 0.06 mm.
Middle unit—bottom	Poorly welded, devitrified groundmass with some shards retaining partial spherical shape. Spherulitically devitrified pumice fragments common. Iron-stained border common on shards. Quartz phenocrysts average 0.6 mm; oligoclase, 0.2 mm.
Lower unit—top	Poorly welded, devitrified groundmass of shards and spherulitically devitrified pumice. Quartz and sanidine phenocrysts range from 0.3 to 0.6 mm.
Lower unit—middle	Moderately welded, devitrified groundmass with minor amounts of spherulitically devitrified pumice. Quartz phenocrysts average 0.3 mm; sanidine, 0.2 mm; oligoclase, 0.1 mm.
Lower unit—bottom	Densely welded, devitrified groundmass with shards flattened parallel to plane of compaction and few spherulitically devitrified pumice fragments. Sanidine phenocrysts average 0.4 mm; oligoclase, 0.2 mm.
Lower unit—vitrophyre	Glassy groundmass of broken shards with perlitic cracks, and devitrified, compressed lithophysae. Quartz phenocrysts average 0.1 mm; sanidine, 0.2 mm. Very minor apatite is 0.3 mm.

all samples with the exception of the basal vitrophyre of the crystal-rich tuff member, for which only total H_2O is given. Normative compositions were calculated from the data with a revised version of the graphic normative analysis program (Stuckless and Van Trump, 1979).

The general chemical homogeneity of the Joe Lott Tuff Member is evident in table 4. Most of the iron is present as Fe^{3+}. The tuff has a high total alkali content ($K_2O + Na_2O$), with a mean value of 8.72 wt percent; K_2O is higher than Na_2O (average K_2O/Na_2O = 1.38). This alkali content is slightly higher than that of average rhyolites (R. W. Le Maitre, written commun., 1983). Agpaitic indices [molar $(Na_2O + K_2O)/Al_2O_3$] for the samples, listed in table 6, are all less than 1, and the lowest samples are hydrated with probable loss of Na. Thus, the Joe Lott Tuff Member is alkali-rich but not peralkaline.

The crystal-rich member has the highest total alkali content (9.96 wt percent) of any of the samples analyzed (table 5). This results from a higher Na_2O content in the crystal-rich member than in the Joe Lott Tuff Member.

Selected major-element concentrations from table 4 are plotted against stratigraphy on figure 9. Analytically significant trends from the basal vitrophyre to the top of the lower cooling unit include a slight increase in SiO_2, MgO, and K_2O, and a small decrease in Al_2O_3, total Fe oxides as Fe_2O_3, and Na_2O. The smooth increase in SiO_2 and K_2O is broken by a slight discontinuity between the bottom and middle of the lower unit. Likewise, the regular decrease in Fe oxides (total) and CaO is broken by a discontinuity at the same stratigraphic position. This stratigraphically coincident discontinuity is exhibited by other elements (below) and suggests a minor perturbation of chemical gradients in the magma chamber or the eruptive mechanism. Analytically significant differences between averages of the lower unit and of other units are minor; however, the pink unit does have a somewhat lower K_2O concentration. The crystal-rich tuff member contains less Si and slightly more Fe oxides (total), Al_2O_3, and CaO than does the Joe Lott Tuff Member.

The concentrations of normative minerals Q, Or, and Ab are plotted versus stratigraphy on figure 10. The Q and Or contents increase upward in the lower cooling unit, mimicking increases in SiO_2 and K_2O (fig. 9). The decrease in Na_2O and in calculated Ab content at the top of the lower cooling unit is not reflected in actual feldspar compositions, and it probably indicates some postemplacement removal of Na_2O from the groundmass.

The abundances of 34 minor and trace elements in the Joe Lott Tuff Member and the basal vitrophyre of the crystal-rich tuff member are listed in table 7. Samples were analyzed for Be, Mo, Li, and Sn by induction-coupled-plasma optical-emission spectroscopy (Taggart and others, 1981) or by semiquantitative 6-step spectrographic analysis. Uranium was determined by a delayed neutron method (Millard and Keaten, 1982). Contents of 21 additional trace elements were measured by instrumental neutron-activation analysis (INAA) (Gordon and others, 1969). Concentrations of Ba and Sr (not determined by INAA) were determined by energy-dispersive X-ray analysis, as were Rb, Nb, and Y. Estimates of analytical precision are listed in table 7 as coefficients of variation (in percent).

Minor- and trace-element abundances in whole rocks are plotted versus stratigraphic position in figure 11. Elements exhibiting similar compositional variations are grouped together, and error brackets indicate estimated analytical precision ($\pm 2\sigma$) for typical values. Common features of these plots that are best documented by analytically significant variations in Co, Mn, Sc, and REE include (1) a trend of element enrichment from the top of the lower cooling unit to its base that suggests roofward enrichment in the magma chamber, (2) a compositional discontinuity within the lower cooling unit that disrupts this trend and that occurs at the same stratigraphic position as the discontinuity previously observed for some major elements (fig. 9), and (3) a compositional discontinuity between the lower and middle cooling unit.

Chondrite-normalized rare-earth-element (REE) patterns (fig. 12) indicate that most of the samples of the Joe Lott Tuff Member have very similar REE abundances and ratios. The exception is the sample from the top of the lower cooling unit (M829), which has significantly lower REE abundances. This observation was confirmed by a subsequent analysis of a separately processed sample from the top of the lower cooling unit. The consistent Ta and Th content but markedly lower Na_2O content of this sample leads us to suspect that some postemplacement alteration has occurred. The basal vitrophyre of the crystal-rich tuff member (M672) has a much higher (two- to three-fold) REE content and a shallower negative Eu anomaly than the Joe Lott Tuff Member.

Enrichment factors (Hildreth, 1977, 1979) calculated for the lower cooling unit (fig. 13) indicate the overall pattern of enrichment and depletion in early-erupted basal vitrophyre compared to the latest erupted top of the unit. Similar enrichment factors reported for early/late units of the Bishop Tuff (Hildreth, 1981) are included for comparison. Starred values are too low for their statistical significance to be assessed with confidence, according to estimates of analytical precision. Enrichments and depletions for the majority of ele-

ments are of the same sense in the Bishop Tuff and Joe Lott Tuff Member, but differ in magnitude. In contrast to the Bishop Tuff, the Joe Lott Tuff shows roofward enrichment of Co, Mn, and the light REE. The high value of Cs is probably due to secondary enrichment (Keith and others, 1983).

PHENOCRYST ABUNDANCES AND COMPOSITIONS

The compositions of phenocrysts in the Joe Lott Tuff Member and the crystal-rich tuff member were studied by analyzing phenocryst separates and polished sections with the electron microprobe. Quartz is the most abundant phenocryst in the Joe Lott Tuff Member; sanidine and oligoclase follow in order of abundance. Hematite was the only iron oxide mineral found in the samples. Biotite, generally oxidized, and augite are found in roughly equal quantities in each of the samples. Accessory apatite, zircon, and sphene occur in order of diminishing abundance. The basal vitrophyre of the Joe Lott Tuff Member contains sparse allanite, chevkinite, hornblende, and fluorite. The crystal-rich tuff member contains approximately 22 volume percent phenocrysts including, in order of decreasing abundance, quartz, sanidine, biotite, secondary hematite, augite, andesine, sphene, zircon, and apatite. As all of the Joe Lott Tuff Member samples contain less than about 1 percent total phenocrysts, statistical counting of the phenocryst population in thin sections would be virtually meaningless. However, as each sample has about the same *total* phenocryst proportion, the *relative* proportions of each minor mineral can best be determined by heavy-mineral separation. These results are reported in table 8.

FIGURE 7 (Above and facing page).—*A*, Pink cooling unit of the Joe Lott Tuff Member showing the two ash-flow tuffs separated by the air-fall layer near the middle of the photograph. Note the characteristic cavernous weathering. Contact with the overlying upper unit is behind telephone pole. *B*, Air-fall layer in the pink cooling unit showing the three graded layers of rhyolite fragments and pumice.

SAMPLE PREPARATION FOR MICROPROBE ANALYSES

Mineral separates of feldspar, zircon, apatite, allanite, chevkinite, amphibole, and pyroxene were analyzed by microprobe. They were separated from the bulk samples as follows:

Samples M827–M833 and M820 were coarsely crushed, and lithic fragments larger than approximately 2 mm were removed by hand. The samples were then pulverized and fed across a Wilfley table in order to separate the predominant (about 99 volume percent) fine-grained devitrified groundmass. The residues remaining on the Wilfley table were sorted according to density using the heavy liquids bromoform and methylene iodide, and the splits obtained were processed by magnetic separator. Sample M672, collected at an earlier date, was treated similarly except sieving replaced the Wilfley table and heavy-mineral separations were performed on the –60 to +120 size fraction.

The minerals to be analyzed by microprobe were mounted in epoxy that filled holes in aluminum or brass discs. The discs served as holders during subsequent polishing.

Microprobe analyses were performed on the U.S. Geological Survey Denver ARLSEMQ microprobe. Electron-beam size was approximately 1 μm in diameter. Background was measured on either side of analytical peaks and then averaged. Reported detection limits were calculated using three times the standard deviation of background counts. Microprobe operating conditions for each mineral are listed in table 9.

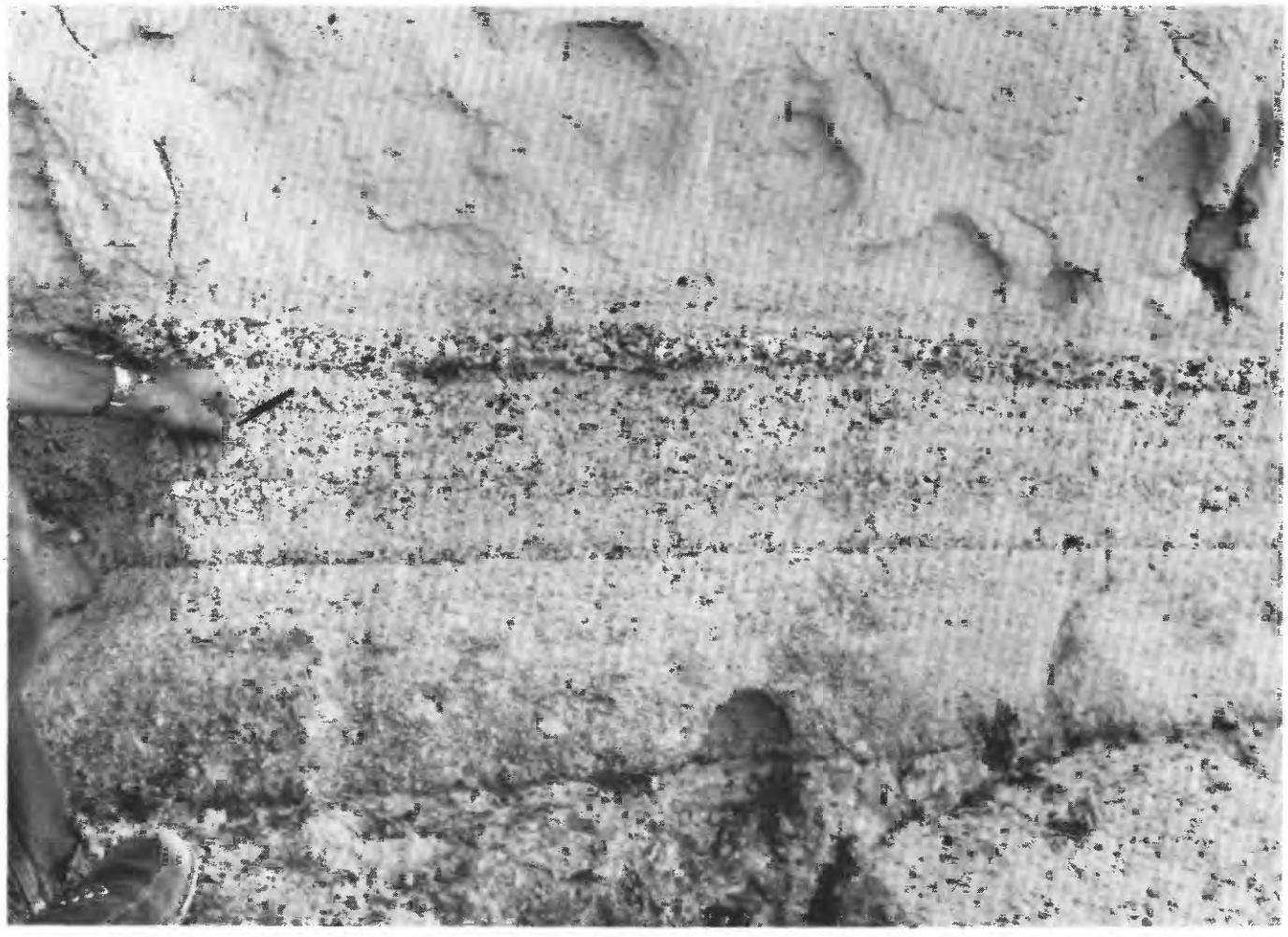

FELDSPAR

Potassium feldspar (sanidine) and, to a lesser extent, plagioclase are present in all phenocryst samples. Clear to white euhedral grains range in size from 170 to 240 μm in their long dimension. Core and rim compositions were determined on randomly selected feldspar separates from each sample. The results for each sample were averaged. Little core- to-rim compositional variation was observed with the exception of potassium feldspar rims on some plagioclase grains in samples M827 and M831. An, Ab, and Or were calculated from CaO, Na_2O, and K_2O contents. To insure that xenocrystic feldspars were not major contaminants of the mineral separates, feldspars within pumice fragments were also probed in polished thin sections. Reasonable agreement was found between data from the grain mounts and the polished thin sections (tables 10 and 11), and similar trends are observed.

ABUNDANCE

Relative abundance of sanidine and plagioclase, per sample, is also listed. Only the mineral-separates data are discussed in subsequent sections as those data are representative of a much larger sample population than the thin-section data. Plagioclase was observed in some thin sections but not in the corresponding mineral separates. The reason for this is not clear.

COMPOSITION

A plot of feldspar compositions on the ternary diagram of figure 14 identifies the feldspars as sodic sanidine and dominantly oligoclase (Deer and others, 1963). Plagioclase in the crystal-rich tuff member is andesine.

Analytically significant changes in sanidine composition are present and vary as a function of stratigraphic position (table 10, fig. 15). In the studied section Or content of sanidine ranges from 61.9 to 33.3 wt percent, Ab content of the same phenocrysts ranges from 38.5 to 63.5 wt percent, and An ranges from 0.7 to 3.7 wt percent. In general, upward in the stratigraphic section, the Or content decreases, and the Ab and An contents increase. A similar decrease in Or content of sanidine with stratigraphic height is reported for the

TABLE 5.—*Major-element analyses (anhydrous, normalized to 100 percent) and CIPW norms of the Joe Lott Tuff Member and the crystal-rich tuff member*

[Analyses in weight percent; D.I., differentiation index; slash (/), not analyzed for; blanks, no information, coefficient of variation (C.V.) in percent. Analysts for samples M820, M827-M833: X-ray fluorescence (XRF) by J. S. Wahlberg, J. Baker, and J. Taggart; titration (TI), Penfield (PEN), gravimetric (GR), carbon elemental analyzer (EA) by H. Heiman, F. E. Lichte, F. Newman, and G. Mason. Analysts for sample M672: rapid rock analysis (RR) by J. Reid]

Sample No.----	M820	M827	M828	M829	M830	M831	M832	M833	M672	Estimated	Analytical methods	
Lab No.-------	D-228264	D-228268	D-228269	D-228270	D-228271	D-228272	D-228273	D-228274	D-215889	C.V.	Joe Lott	M672
SiO_2----------	75.85	76.64	76.02	77.31	76.65	76.56	76.57	76.11	71.44	0.26	XRF	RR
Al_2O_3---------	13.21	12.57	12.53	12.26	12.76	12.90	13.31	12.77	14.72	.40	XRF	RR
Fe_2O_3---------	.87	.91	.98	.92	.78	.93	.84	.91	1.24	.27	XRF	RR
FeO----------	.26	.01	.01	.01	.09	.01	.11	.09	.58		TI	RR
MgO----------	.21	.20	.31	.42	.21	.20	.60	.20	.36	.66	XRF	RR
CaO----------	.80	.40	.99	.59	.36	.34	.75	.35	1.14	.27	XRF	RR
Na_2O----------	3.80	3.85	3.86	2.81	3.50	3.76	3.51	4.22	4.98	2.89	XRF	RR
K_2O----------	4.77	5.15	5.10	5.57	5.49	5.12	4.12	5.15	4.98	.32	XRF	RR
TiO_2----------	.15	.11	.13	.11	.11	.12	.12	.13	.36	.76	XRF	RR
P_2O_5----------	<.1	.10	<.1	<.1	<.1	<.1	<.1	<.1	.07	.93	XRF	RR
MnO----------	.07	.05	.06	<.02	.05	.06	.07	.06	.11	1.87	XRF	RR
LOI----------	4.05	1.14	3.59	3.02	1.49	.78	5.42	1.06	/		XRF	
H_2O^+----------	2.82	.34	1.49	.91	.90	.39	3.41	.23	2.5	4	PEN	RR
H_2O^-----------	.68	.33	.86	1.02	.49	.20	1.49	.10	.36	10	GR	RR
CO_2----------	.01	<.01	<.01	<.01	<.01	.04	.01	.01	.18		EA	RR

TABLE 5.—*Major-element analyses (anhydrous, normalized to 100 percent) and CIPW norms of the Joe Lott Tuff Member and the crystal-rich tuff member*—Continued

Sample No. **Lab No.**	M820 D-228264	M827 D-228268	M828 D-228269	M829 D-228270	M830 D-228271	M831 D-228272	M832 D-228273	M833 D-228274	M672 D-215889
Normative minerals (weight percent, calculated without H_2O and CO_2)									
Q	33.42	33.66	32.13	37.79	34.20	34.10	37.87	31.02	21.11
C	.32	.18		.54	.40	.57	1.71		
Or	28.22	30.43	30.11	32.91	32.47	30.24	24.36	30.42	29.41
Ab	32.18	32.60	32.70	23.74	29.60	31.79	29.74	35.73	42.12
An	3.98	1.30	1.80	2.94	1.79	1.66	3.70	.68	3.14
Wo			1.24					.44	.86
En	.53	.51	.78	1.04	.51	.51	1.49	.50	.90
Mt	.66				.14		.25	.11	1.19
Hm	.41	.91	.98	.93	.69	.93	.67	.84	.42
Il	.28	.13	.16	.02	.22	.15	.22	.25	.69
Tn			.11						
Ru		.04		.10		.04			
Ap		.24							.17
Total	100.00	100.01	100.00	100.00	100.00	100.00	100.00	100.00	100.01
Salic	98.12	98.18	96.74	97.92	98.45	98.37	97.38	97.86	95.77
Femic	1.88	1.83	3.27	2.09	1.55	1.63	2.63	2.14	4.24
D.I.	93.82	96.69	94.94	94.44	96.26	96.14	91.96	97.18	92.64

TABLE 6.—*Agpaitic indices [molar $(Na_2O + K_2O)/Al_2O_3$] of the Joe Lott Tuff Member and the crystal-rich tuff member*

Sample	Description	Index
M672	Crystal-rich tuff member, vitrophyre	0.922
	Joe Lott Tuff Member	
M833	Upper unit	0.980
M832	Pink unit	0.769
M831	Middle unit--top	0.909
M830	Middle unit--bottom	0.917
M829	Lower unit--top	0.868
M828	Lower unit--middle	0.947
M827	Lower unit--bottom	0.948
M820	Lower unit--vitrophyre	0.865

Bandelier Tuff (Smith and Bailey, 1966). An apparent discontinuity in the plots of sanidine composition versus stratigraphic height occurs in the lower unit. The affected interval is the same as that identified on the basis of anomalous whole-rock chemistry (figs. 9 and 11).

Compositional changes in plagioclase as a function of stratigraphic position include variations in An content from 11.8 to 29.3 wt percent, and corresponding variations in Ab from 81.3 to 66.9 wt percent and in Or from 6.9 to 3.3 wt percent (table 10, fig. 16). Upward in the stratigraphic section, An content of the plagioclase increases, and Ab and Or contents decrease. Plagioclase is absent in the feldspar separates from the basal vitrophyre, bottom of the middle unit, pink, and upper units.

The compositions of plagioclase found in the thin-section samples but not in the mineral separates from those samples (M820, M830, M832) are shown as circles on figure 16. These data support a smoother increase in An content and decrease in Ab content upward through the lower and middle cooling units than would be the case if the thin-section data were not used. The composition of the plagioclase found in the pink unit is fairly close to that of the plagioclase in the top of the middle unit.

The percentage abundance of sanidine versus total feldspar in the feldspar separates (fig. 17) steadily decreases from about 100 to 50 percent going upward in the lower cooling unit. This decrease in the sanidine component has also been observed during the progressive eruption of many other large volume (100–1,000 km^3) silicic magma chambers (Hildreth, 1981). Reequilibration of the magma chamber is clearly shown by return to a sanidine content of 100 percent of total feldspar at in the bottom of the middle unit. The pink and upper units both contain 100 percent sanidine. The basal vitrophyre of the crystal-rich tuff member has 85 percent sanidine.

STRUCTURAL STATE

X-ray diffraction measurements of alkali feldspar powders from the crystal-rich tuff member (samples M74 and M75) provided 2θ values that were used to estimate structural state and composition according to the method outlined by Wright (1968). Measured 2θ values are as follows:

	$\bar{2}04$	060
M74	51.13°	41.90°
M75	51.16°	41.93°

These 20 values are plotted on figure 18 and indicate a high or disordered structural state and a composition intermediate between the potassic and sodic end members.

ZIRCON

Two populations of zircons are present in each sample: large (230 μm long) clear grains and small (110 μm) pink grains. Both types occur as dipyramidal euhedra.

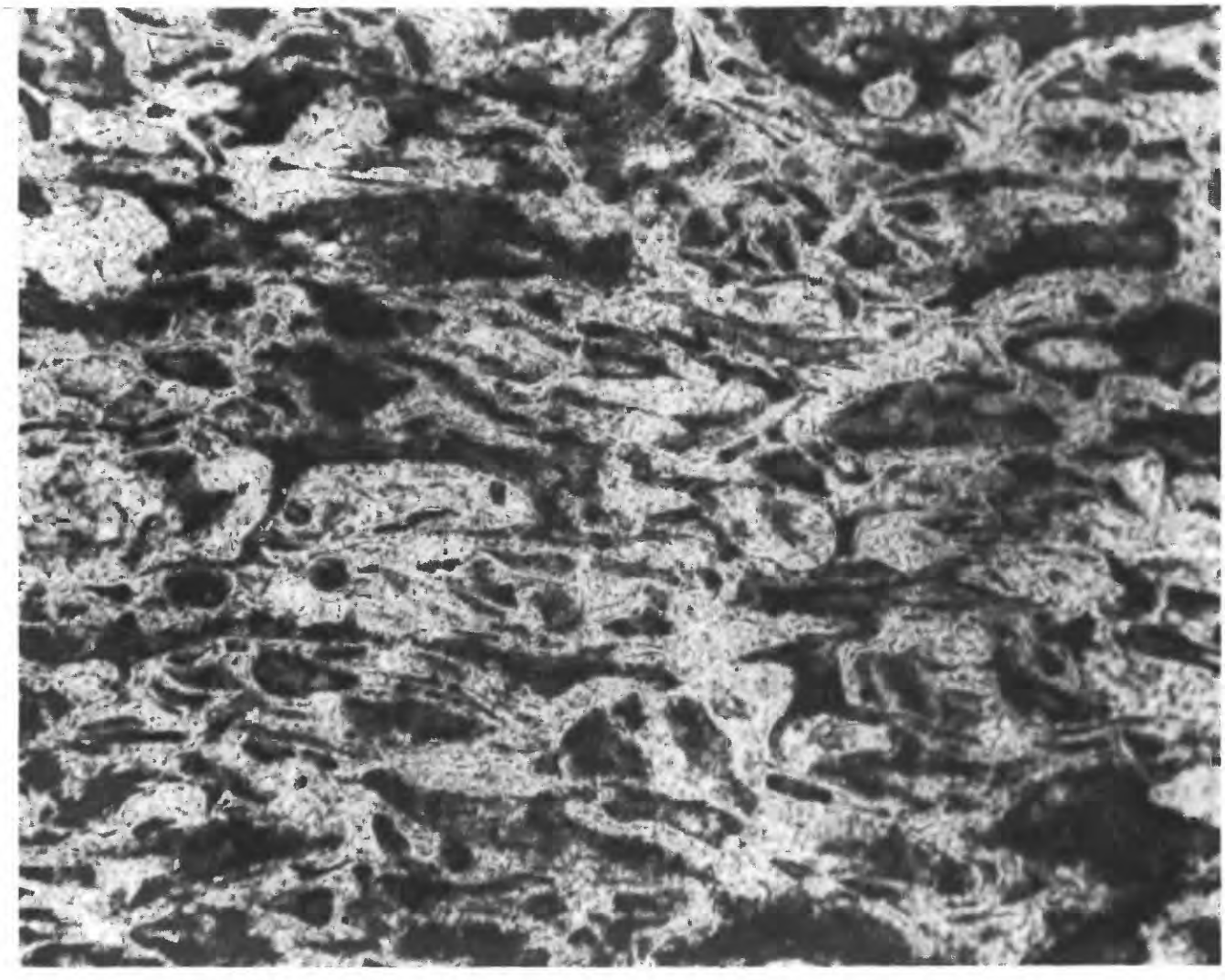

FIGURE 8.—Densely welded base of the lower cooling unit of the Joe Lott Tuff Member. Glass shards are flattened parallel to the plane of compaction. Field of view is 1.8 by 1.4 mm.

Cores and rims of ten grains from both populations in all samples were analyzed by microprobe. Concentrations of ZrO_2, HfO_2, and SiO_2 in each sample are homogeneous and were averaged. Concentrations of UO_2 and REE in each sample are variable. Analyses above detection limits were averaged for each sample and are given in table 12, along with a fraction indicating the ratio of the number of detected values to the total number of analyzed zircons. Concentrations of P_2O_5 and Pr_2O_3 are below calculated detection limits in all samples.

Owing to the severe mutual interference problems involved in analyzing the REE, particularly the heavy ones, spectrum stripping was employed. In this procedure, counts were recorded on the analytical peak of each element, its background, and on the analytical peaks of interfering elements in a standard of known concentration. Standards were used to determine the contribution of known concentrations of interfering elements to a particular analytical peak. Peak and background counts for each element were determined on the unknowns. The same spectrometer was used to insure similar operating conditions during measurement of both the element and its interfering element. After subtracting the contributions of background and the interfering element from the analytical peak, calibration curves plotting corrected intensity versus concentration were established.

A test using spectrum stripping on the data for the basal vitrophyre indicated that all REE other than La and Ce were below detection limits. Subsequent analyses were attempted only for La and Ce.

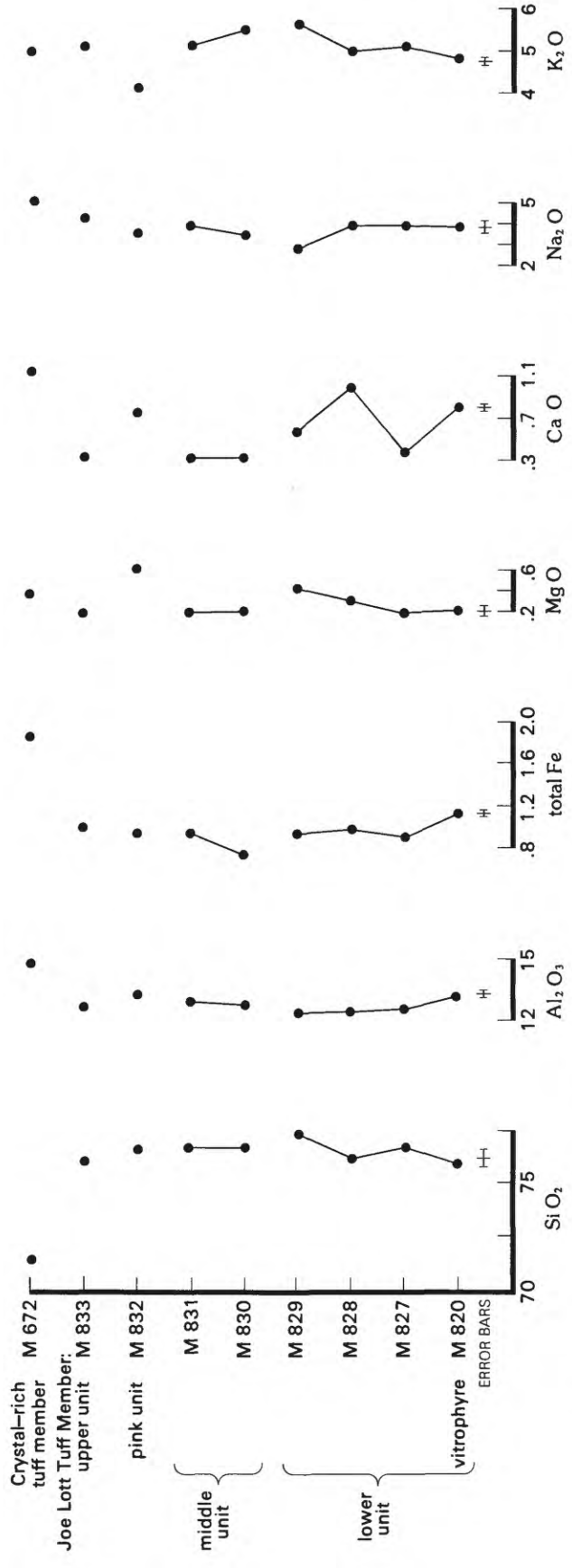

FIGURE 9.—Major-element composition of whole-rock samples (anhydrous, normalized to 100 percent) plotted versus stratigraphic position. Estimates of analytical precision are shown by error bars that delimit $\pm 2\sigma$ about a typical value.

TABLE 7.—*Minor- and trace-element analyses of the Joe Lott Tuff Member and the crystal-rich tuff member*

[Analyses in parts per million, except those for F, Cl, and S, which are in weight percent. Slash (/), not analyzed for; leaders (—), below detection limit; coefficient of variation (C.V.) in percent. Analysts for specific ion electrode (IE), sulfur elemental analyzer (EA), and induction-coupled-plasma optical-emission spectroscopy (ICP), H. Heiman, F. E. Lichte, F. Newman, and G. Mason; delayed neutron activation (DNA) by R. Bies, H. T. Millard, Jr., B. Keaten, M. Coughlin, and S. Lasater; energy dispersive X-ray analysis (EDX) by K. Budding; instrumental neutron activation analysis (INAA) by J. Budahn and R. Knight. Analytical method for M672 listed where different: rapid rock analysis (RR) by J. Reid; semiquantitative 6-step spectrographic analysis (SQS) by M. J. Malcolm]

	M820	M827	M828	M829	M830	M831	M832	M833	M672	Estimated C.V.	Analytical method Joe Lott	Analytical method M672
F	0.11	0.03	0.03	0.15	0.03	0.03	0.14	0.04	0.12	7	IE	RR
Cl	/	/	/	/	/	/	/	/	.03			RR
S	<.01	<.01	<.01	<.01	<.01	<.01	<.01	.02	/		EA	
U	13.1	9.67	8.69	6.55	9.34	10.1	11.7	8.91	9.69	3	DNA	
Be	6	6	7	5	6	6	6	6	7	10	ICP	SQS
Li	40	36	40	20	38	50	39	40	/	10	ICP	
Mo	7	4	4	2	3	4	9	<2	5	10	ICP	SQS
Sn	11	<10	<10	20	<10	<10	<10	<10	/	10	ICP	
Ba	95	57	76	75	53	67	80	78	437	10	EDX	
Co	.84	.34	.49	.30	.29	.39	.34	.75	.70	1-4	INAA	
Cr	2.89	<2.2	1.42	1.26	<.50	1.3	--	2.37	1.09	2-16	INAA	
Cs	19.2	4.69	4.19	2.17	4.64	3.99	12.5	3.03	18.2	5-8	INAA	
Hf	5.47	5.57	5.39	5.42	5.44	5.69	5.66	5.50	9.19	1-2	INAA	
Mn	561	478	506	99.8	433	564	613	542	581	1	INAA	
Nb	39	43	39	38	44	45	42	38	39	5	EDX	
Rb	304	283	264	278	310	285	271	240	305	5	EDX	
Sb	.56	.34	.34	1.8	.21	.38	.37	.30	.30	1-10	INAA	
Sr	50	49	168	47	121	28	50	36	120	5	EDX	
Ta	3.18	3.29	3.11	3.29	3.19	3.35	3.34	3.23	3.42	1-2	INAA	
Th	35.8	36.7	35.4	35.3	36.9	37.5	36.9	36.5	28.7	1	INAA	
Y	12	13	16	19	20	19	22	21	31	5	EDX	
Zr	130	138	129	135	126	154(EDX)	156(EDX)	136	337	1-2	INAA	
Sc	2.09	1.70	1.80	1.47	1.70	1.81	1.79	2.01	4.44	1-2	INAA	
La	41.9	43.7	42.3	35.9	41.2	42.9	42.1	42.6	73.1	1	INAA	
Ce	67.5	69.5	67.7	58.6	68.8	70.2	70.1	70.8	147	1-2	INAA	
Nd	18.9	19.9	20.9	16.3	18.4	18	18.7	20.4	57.4	2-7	INAA	
Sm	3.02	2.84	2.78	2.44	2.88	2.84	2.86	2.98	9.67	1-5	INAA	
Eu	.284	.209	.239	.208	.201	.229	.213	.270	1.44	1-3	INAA	
Gd	--	--	--	--	--	--	--	--	7.10	6	INAA	
Tb	.406	.366	.388	.289	.379	.377	.380	.411	1.10	1-3	INAA	
Dy	2.76	2.53	2.49	2.28	2.72	2.36	2.40	2.65	5.24	2-11	INAA	
Tm	--	--	--	--	--	--	--	--	.483	8	INAA	
Yb	2.22	2.14	2.28	2.03	2.24	2.25	2.28	2.18	3.43	1	INAA	
Lu	.310	.370	.380	.340	.370	.370	.370	.380	.550	1-4	INAA	

Selected oxide concentrations in the zircons are plotted against stratigraphy on figure 19. Within each sample, the composition of zircons is generally homogeneous with slight variations. The pink color of zircons has been associated with increased structural damage due to higher U concentration or greater age (C. W. Naeser, personal commun., 1982). Limited microprobe data indicate that the pink zircons in the bottom and middle of the lower cooling unit have a higher U content than coexisting white zircons (fig. 19).

The SiO_2, ZrO_2, and HfO_2 contents of zircons are fairly uniform throughout the Joe Lott Tuff Member. The drop in Zr/Hf of clear zircons from the basal vitrophyre through the middle of the lower cooling unit

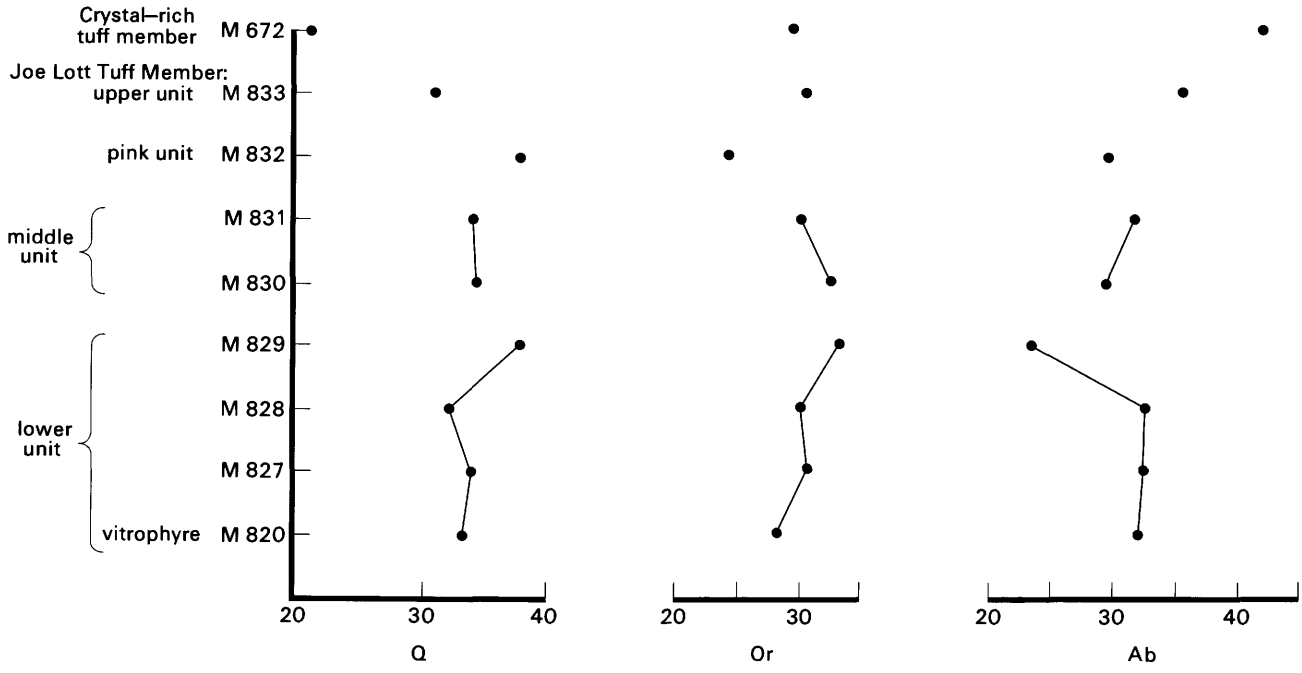

FIGURE 10.—Normative abundances of Q, Or, and Ab (as weight percent) plotted versus stratigraphic position.

TABLE 8.—*Relative percentages of minor mineral phases in the Joe Lott Tuff Member and the crystal-rich tuff member. Data obtained by grain estimates of mineral separates*

[Leaders (—), none. Note difference between these abundances and modal analyses in table 4]

Sample	Total percent phenocrysts*	Hematite	Pyroxene	Biotite	Sphene	Apatite	Zircon	Allanite and chevkinite	Fluorite
Crystal-rich tuff member,									
vitrophyre----------	21.9	28	17.0	52.0	2.0	0.1	0.6	---	---
Joe Lott Tuff Member									
Upper unit----------	1.0	57	8.0	11.0	.4	1.0	.6	---	---
Pink unit----------	.7	73	15.0	7.0	2.0	2.0	1.0	---	---
Middle unit--top------	1.0	97	2.0	---	.1	.2	1.0	---	---
Middle unit--bottom---	.4	50	14.0	18.0	.2	18.0	.5	---	---
Lower unit--top-------	3.1	93	3.0	2.0	.2	.2	2.0	---	---
Lower unit--middle----	.7	90	.1	8.0	---	1.0	1.0	---	---
Lower unit--bottom----	.6	86	4.0	6.0	.3	3.0	1.0	---	---
Lower unit--Vitrophyre	.3	88	6.0	.7	.7	2.5	1.2	0.5	0.3

*Total percent phenocrysts as determined by modal abundance in thin section. From table 4.

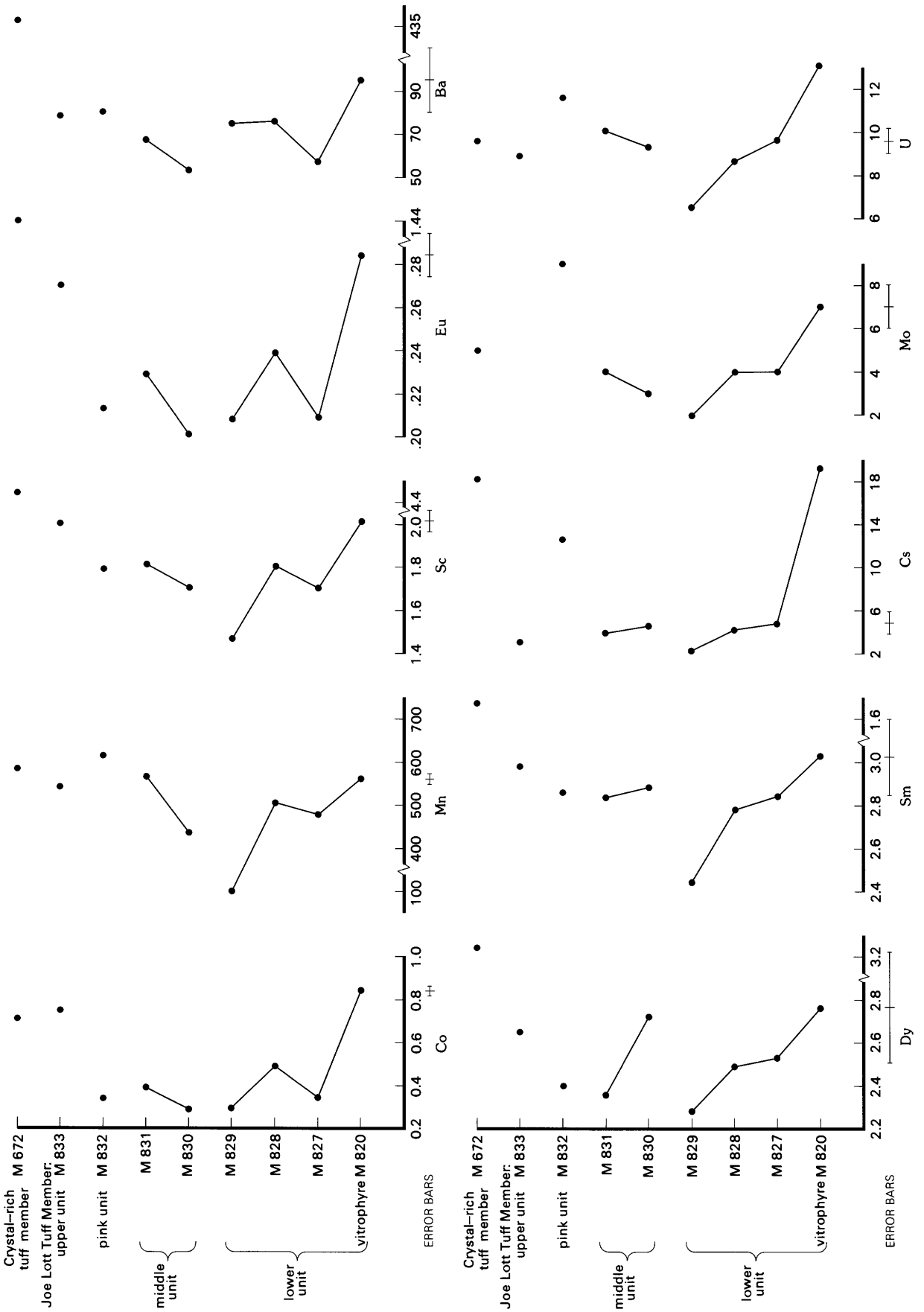

FIGURE 11.—Minor- and trace-element composition of whole-rock samples plotted versus stratigraphic position. All concentrations are given in parts per million by weight, except those for F, Cl, and S, which are in weight percent. Missing data include undetected and unanalyzed values. Estimates of analytical precison are shown by error bars that delimit $\pm 2\sigma$ about a typical value.

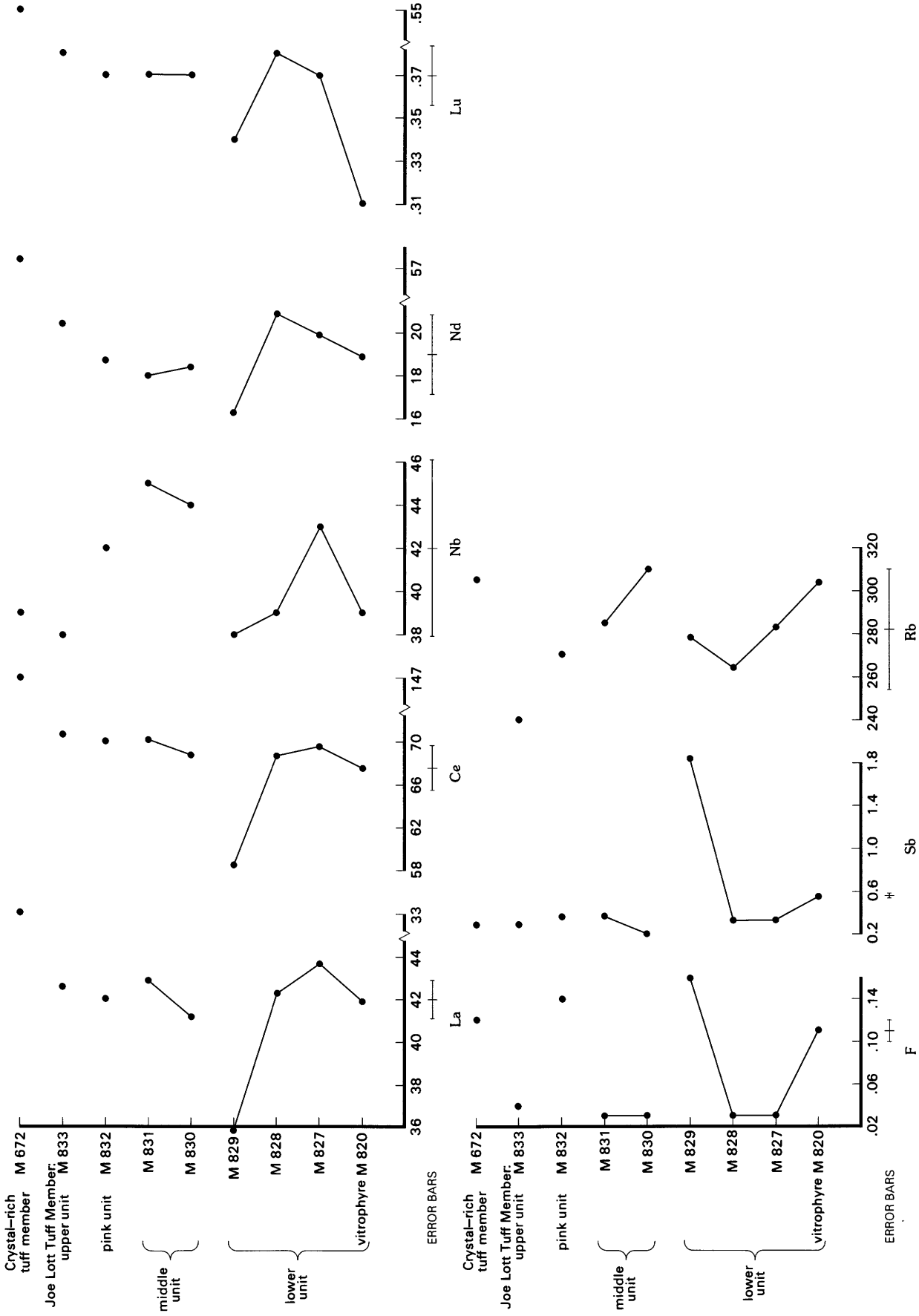

FIGURE 11.—Continued.

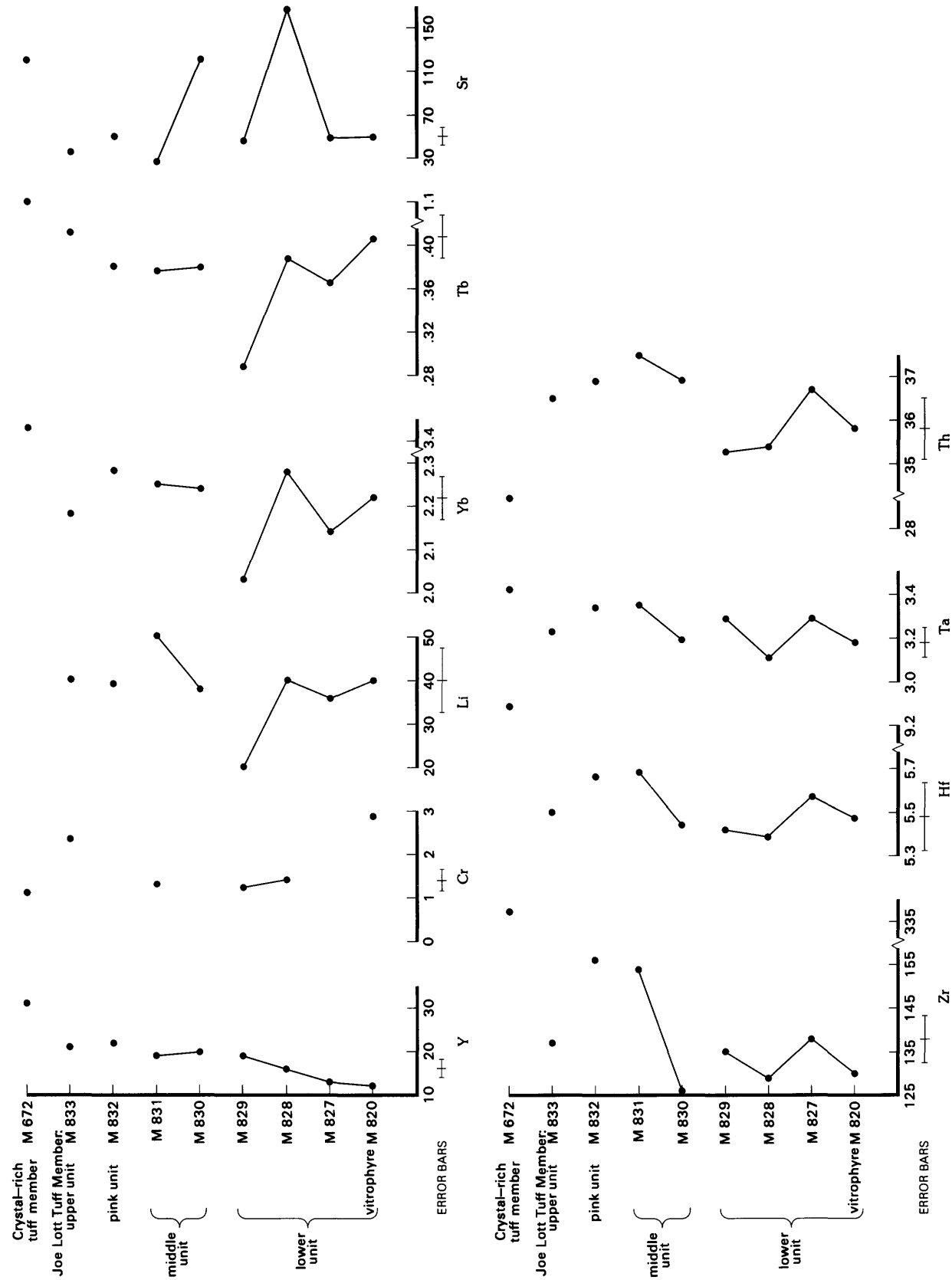

FIGURE 11.—Continued.

TABLE 9.—*Microprobe operating conditions*
[Current for all analyses was 10 nA on brass]

Mineral analyzed	Accelerating voltage	Method of data reduction
Feldspar	10 kv	Bence-Albee
Zircon	20 kv	MAGIC
Apatite	15 kv	MAGIC
Allanite	15 kv	MAGIC
Chevkinite	15 kv	MAGIC
Amphibole	15 kv	Bence-Albee
Pyroxene	15 kv	Bence-Albee

The following standards were used:

Mineral analyzed	*Standards*
Feldspar	Amelia albite (Na), Clear Lake plagioclase (Si, Al, Ca), Benson orthoclase (K)
Zircon	Ceylon zircon (Si, Zr, Hf), euxenite (U), Durango apatite (P, La), REE standard 3 (Drake and Weill, 1972; Y, Ce, Pr)
Apatite	Durango apatite (F, P, Ca), Lemhi biotite (Cl), fayalite (Mn), USGS synthetic glass (Mg), REE standard 2 (Nd), REE standard 3 (Pr, Ce, Y, La)
Allanite and chevkinite	Dolomite (Mg), Wilberforce apatite (F, Na), Peerless apatite (P, Mn), biotite (Fe), sphene (Ca, Ti), REE standard 2 (Nd, Sm), REE standard 3 (Al, Y, La, Ce, Pr), Ceylon zircon (Si), ThO_2 pure (Th), uraninite (U)
Amphibole and pyroxene	USGS synthetic glass (Na, Al, Fe, K, Ca), orthopyroxene (Si, Mg, Mn, Ti, Cr)

is due to a slight systematic rise in Hf content. The ratio drops off for both species of zircons in higher parts of the stratigraphic section through the top of the middle cooling unit, again in response to decreasing Hf content.

The Y content of both the pink and clear zircons increases in the lower cooling unit and, at higher stratigraphic levels, remains high in the pink grains. The pink zircons, which contain more U, apparently also contain more Y.

Fission-track radiography was used to measure the distribution of U in the same zircon samples that were analyzed by microprobe. The pink zircons contain a higher concentration of U than do the clear zircons. The distribution of U is more heterogeneous in the pink zircons, many of which show U-rich rims (fig. 20).

Microprobe analysis of REE in the zircons did not give satisfactory results. Concentrations of La and Ce were not detected in enough samples for the REE abundance to be related to stratigraphy. Detectable concentrations of La and Ce are more common in the pink than the clear zircons; thus, the behavior of La and Ce parallels the apparent behavior of Y and U. The average sum of the detected (La and Ce) is 0.33 wt percent.

Although only minor compositional variation is indicated by the microprobe data, element ratios—when normalized and plotted on a ternary diagram—accentuate chemical distinctions between clear and pink zircons (fig. 21). Effinroff (1972) used Th/Zr, Hf/Zr, and Y/Zr to identify chemical differences among zircons of different crystal habits.

The clear zircons have a higher Hf/Zr ratio and a lower Y/Zr ratio than the pink zircons. With the exception of the pink zircons of M827 and M828, which are exceptionally high in U, the U/Zr of the zircons does not vary much. The clear zircons from the crystal-rich tuff member (M672) are chemically different from the clear zircons in the Joe Lott Tuff Member. Tie lines connecting coexisting zircons indicate that although there are chemical differences from one pair to the next, the differences are not consistent.

APATITE

Apatite forms clear to orange prismatic crystals, 140–280 μm long, commonly terminated by pyramids and

TABLE 10.—*Microprobe analyses of feldspar separates from the Joe Lott Tuff Member and the crystal-rich tuff member*

[Analyses in weight percent; plagioclase not present in all samples]

Sample	Description	Sanidine				Plagioclase			
		Relative proportion (in percent)	An	Ab	Or	Relative proportion (in percent)	An	Ab	Or
M672	Crystal-rich tuff member, vitrophyre--	85	4.4	57.5	38.1	15	35.8	59.3	4.9
	Joe Lott Tuff Member								
M833	Upper unit----------	100	3.2	63.5	33.3				
M832	Pink unit----------	100	2.7	63.0	34.3				
M831	Middle unit--top----------	93	2.8	56.6	40.6	7	29.3	66.9	3.8
M830	Middle unit--bottom----------	100	.7	41.0	58.3				
M829	Lower unit--top----------	50	2.3	44.0	53.7	50	24.9	71.8	3.3
M828	Lower unit--middle----------	60	1.0	37.1	61.9	40	20.3	75.2	4.5
M827	Lower unit--bottom----------	93	3.7	57.0	39.3	7	11.8	81.3	6.9
M820	Lower unit--vitrophyre----------	100	.7	38.5	60.8				

TABLE 11.—*Microprobe analyses of feldspar present in thin sections of the Joe Lott Tuff Member and the crystal-rich tuff member*

[Analyses in weight percent; plagioclase not present in all samples]

Sample	Description	Sanidine				Plagioclase			
		Relative proportion (in percent)	An	Ab	Or	Relative proportion (in percent)	An	Ab	Or
M672	Crystal-rich tuff member, vitrophyre--	88	3.1	53.5	43.4	12	29.5	65.2	5.3
	Joe Lott Tuff Member								
M833	Upper unit----------	100	2.9	63.0	34.1				
M832	Pink unit----------	57	1.9	45.2	52.9	43	24.5	70.1	5.4
M831	Middle unit--top----------	67	1.5	43.7	54.8	33	24.7	69.6	5.7
M830	Middle unit--bottom----------	50	0.7	39.7	59.6	50	19.4	74.7	5.9
M829	Lower unit--top----------	43	1.3	44.2	54.5	57	17.7	74.0	8.3
M828	Lower unit--middle----------	78	0.9	39.9	59.2	22	11.6	82.2	6.2
M827	Lower unit--bottom----------	71	2.9	53.4	43.7	29	19.8	74.7	5.5
M820	Lower unit--vitrophyre----------	33	1.0	51.5	47.5	67	23.0	72.5	4.5

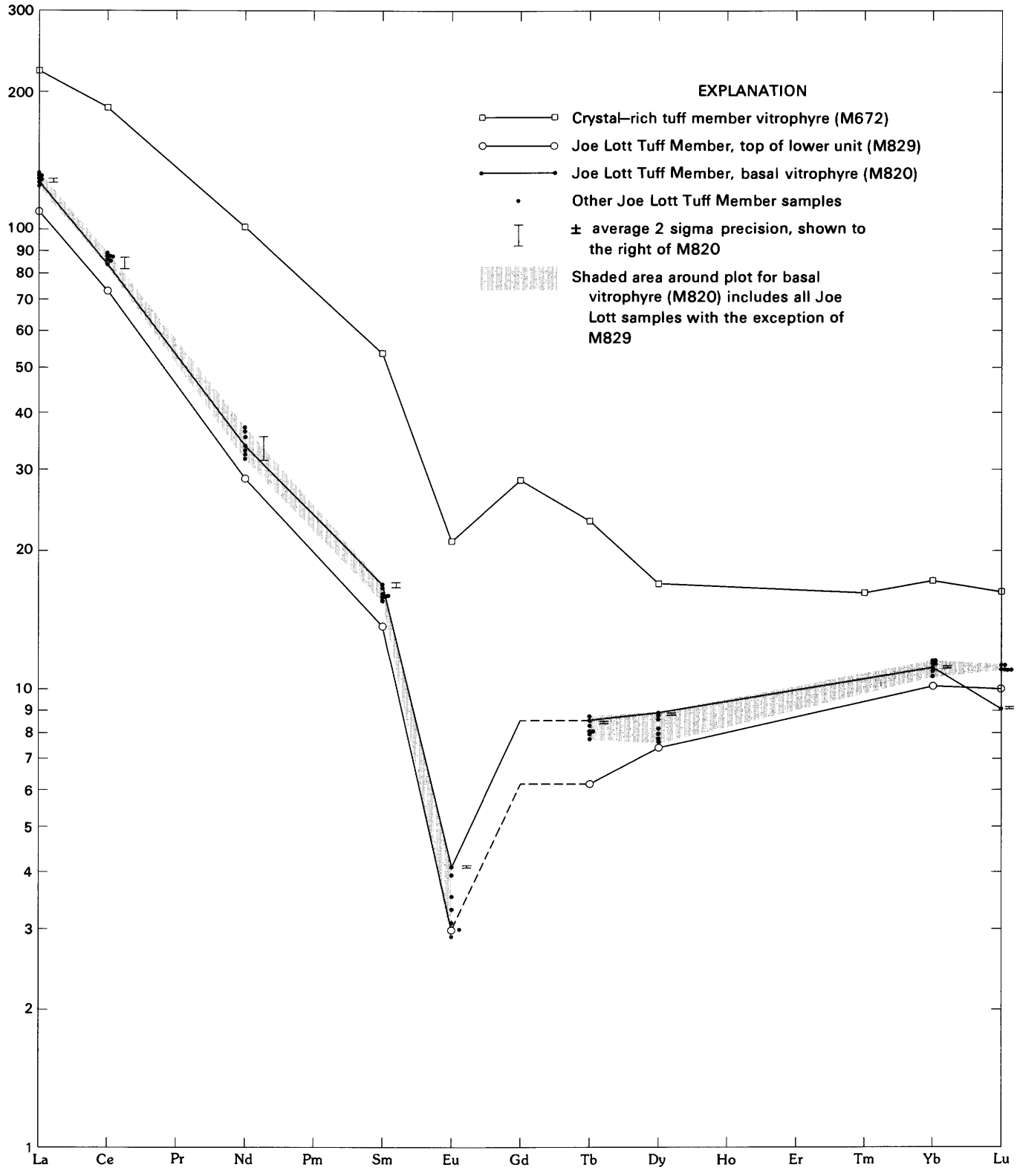

FIGURE 12.—Chondrite-normalized REE patterns in samples of the Joe Lott Tuff Member and the crystal-rich tuff member. Shaded region about the plot for the basal vitrophyre (M820) includes all Joe Lott samples with the exception of the top of the lower unit (M829), which is plotted separately.

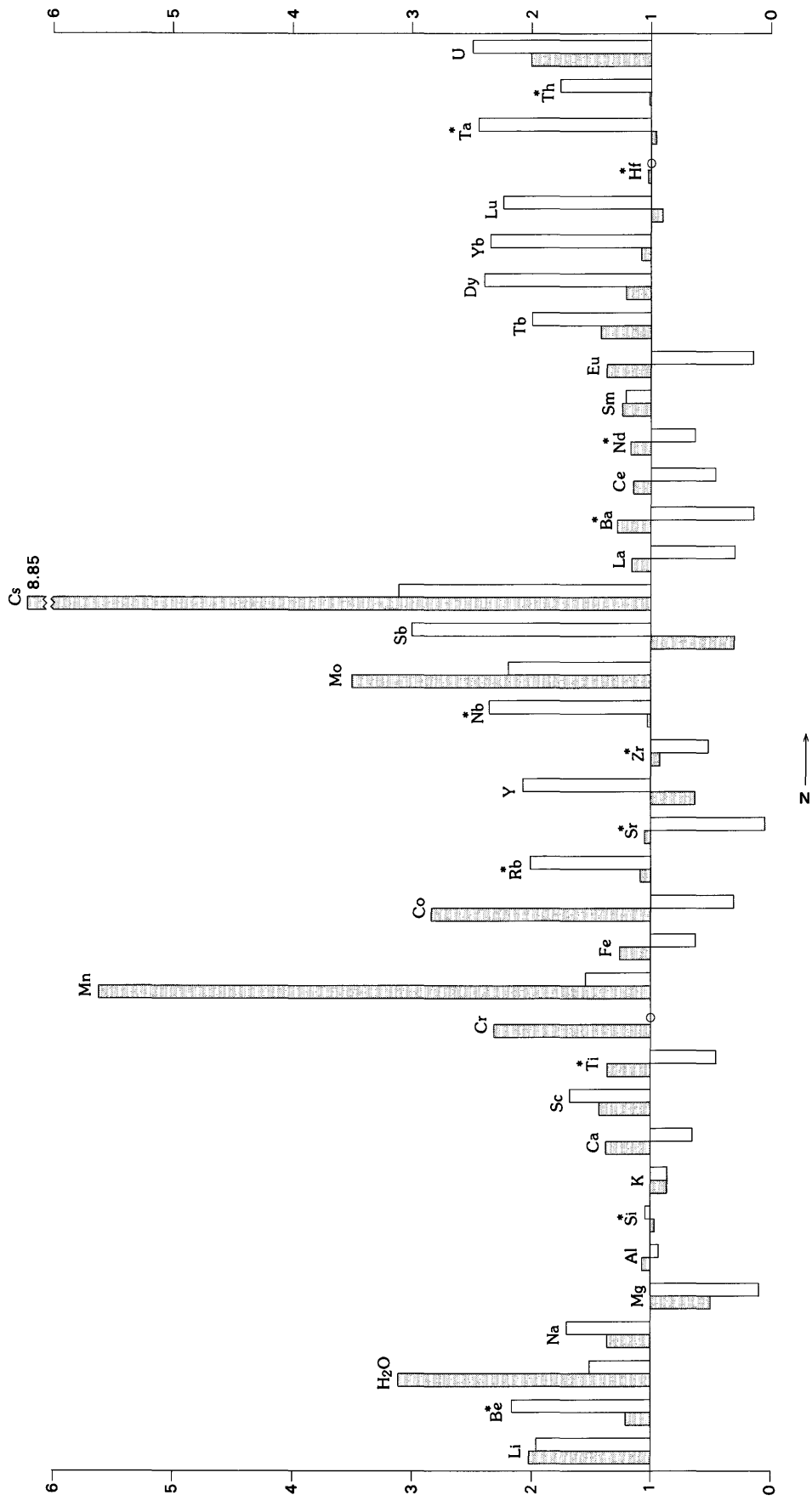

FIGURE 13.—Calculated enrichment factors (concentrations in early erupted rocks/concentrations in late-erupted rocks) for the lower cooling unit of the Joe Lott Tuff Member (black), compared to those of the Bishop Tuff (clear) (Hildreth, 1981). Elements marked by a circle on the line are neither enriched nor depleted. Starred values are too low for their statistical significance to be assessed with confidence, on the basis of estimates of analytical precision.

basal pinacoids. The core and rims of five grains from each sample were analyzed by microprobe (table 12). Concentrations of Cl, F, Nd_2O_3, Pr_2O_3, Ce_2O_3, La_2O_3, Y_2O_3, MgO, and MnO ranged from above to below detection limits. The detected values for these elements are averaged and listed along with the total number of analyses made in table 13. The average sum of the detected REE is 1.33 wt percent (La + Ce + Pr + Nd).

Apatite compositions versus stratigraphy are plotted on figure 22. Analytically significant variations are documented by some elements throughout the lower cooling unit and in the middle unit. The concentrations of P and Mn all increase upward in the lower cooling unit, whereas Cl and Ca decrease. All these elements exhibit discontinuous behavior in their overall trend. Between the lower and middle cooling units, the content of P, Ce, and La all drop and then rise again at the base of the middle cooling unit. Nd, Ce, and La all show a small increase between the pink and upper units.

Some elements, such as Cl, F, Ca, and Mn reverse their concentration trends within the lower cooling unit. The concentration trend in the middle tuff unit is usually the same as the overall concentration trend in the lower unit; a notable exception is Ca.

ALLANITE AND CHEVKINITE

Approximately 50 euhedral crystals of dark-reddish-brown and black allanite, an epidote mineral rich in REE, and (or) chevkinite, an iron-bearing titanosilicate containing REE, were found in the sample of the basal vitrophyre of the Joe Lott Tuff Member, sample M820. The stubby prisms range in size from 60 to 120 μm in length. Owing to the small sample size, 15 of the larger grains were analyzed by electron microprobe rather than by neutron activation. Both the core and rim of the grains were analyzed, but no analytically significant zoning was observed. The results are summarized in tables 14 and 15. Concentrations of F, Na, P, certain REE, and U are below detection limits in the allanite, and Na, P, Mn, some REE, and U are below detection limits in the chevkinite. The 15 grains were identified on the basis of chemistry and X-ray diffraction data as allanite (5) and chevkinite (10). Spectrum stripping was used to determine the concentrations of all REE except La, Ce, and Sm. Concentrations of Tb through Lu were below limits of detection.

The average sum of the light and middle REE in allanite is approximately 21 wt percent (La + Ce + Pr + Nd + Eu + Gd). This is 60 times greater than the light REE concentration (La + Ce) in coexisting zircon and 16 times greater than the concentration of light REE (Nd + Pr + Ce + La) in coexisting apatite.

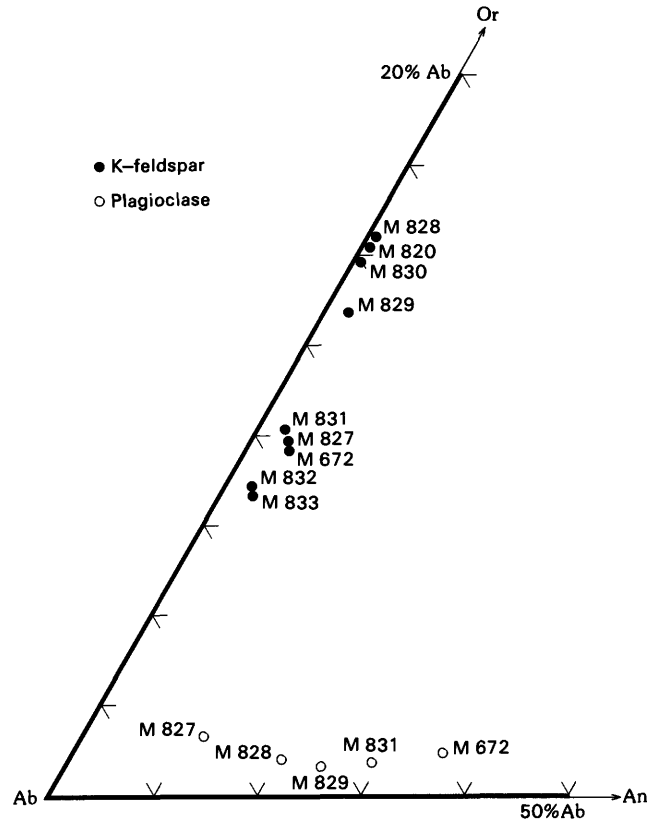

FIGURE 14.—Normative abundances of Or, Ab, and An (as weight percent) in feldspars of the Joe Lott Tuff Member and the crystal-rich tuff member.

The sum of the measured REE in the chevkinite averages about 36 wt percent (La + Ce + Pr + Nd + Sm + Eu + Gd). This is just over 100 times more than in coexisting zircon and 28 times more than in coexisting apatite. Relative to coexisting amphibole and pyroxene, chevkinite is enriched in Ti and depleted in Fe, Mg, Ca, and Al (amphibole only).

PYROXENE

Abundant pale-green pyroxene euhedra are present in all the samples. Slightly larger grains (410 μm long) occur in devitrified samples at or near the bottom of the lower and middle units (M827, M830). Smaller grains (average 200 μm) occur in the remaining sampled units. Pyroxene in the middle (bottom), pink, and upper unit is generally somewhat oxidized; only relatively unaltered grains were selected for microprobe analysis.

Cores and rims were analyzed on five grains from each sample. No analytically significant zonation within crystals was observed. The results were averaged for each sample and, along with the structural formulae, are given in table 16. Table 17 lists the calculated end members (Fe and Mn values assigned to ferrosilite),

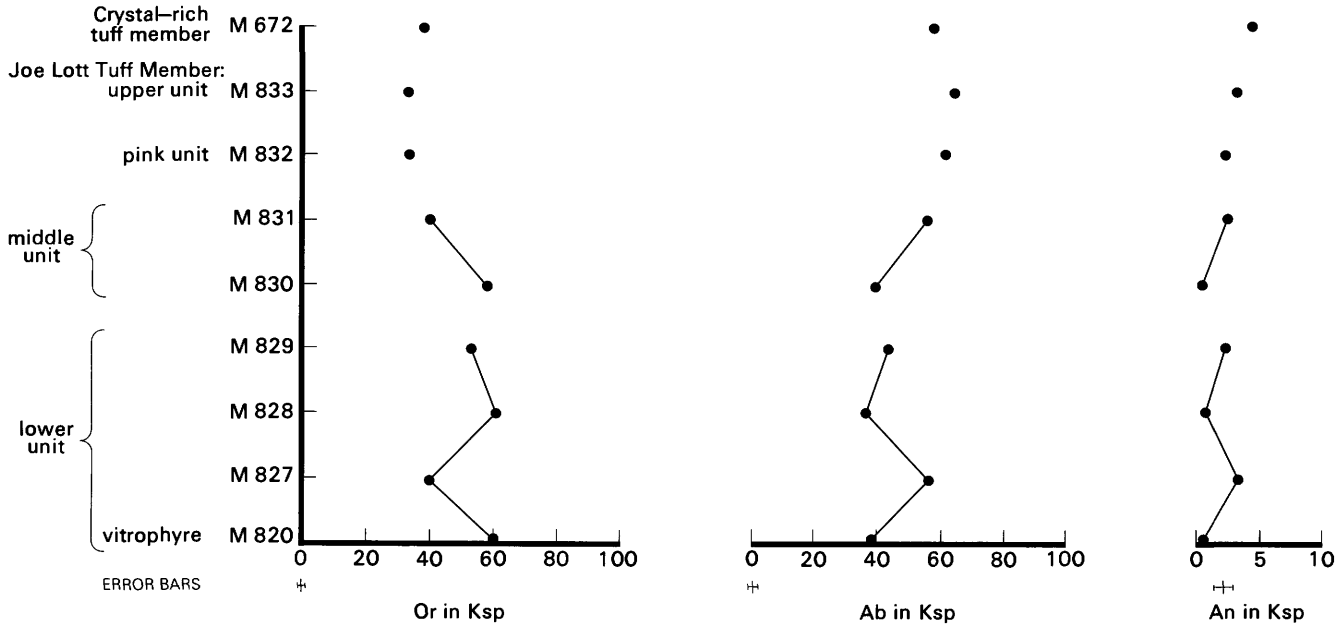

FIGURE 15.—Normative abundances of Or, Ab, and An (as weight percent) in sanidine plotted as a function of stratigraphic position in the Joe Lott Tuff Member and the crystal-rich tuff member. Error bars show average $\pm 2\sigma$ precision.

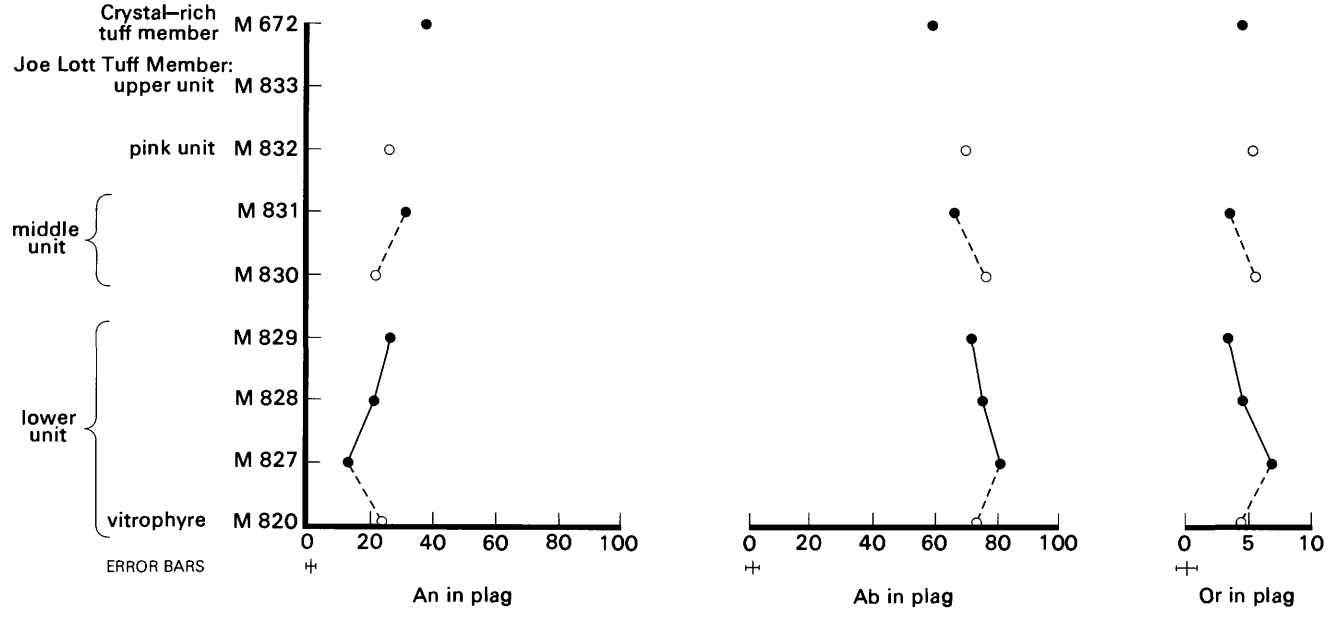

FIGURE 16.—Normative abundances of Or, Ab, and An (as weight percent) in plagioclase plotted as a function of stratigraphic position in the Joe Lott Tuff Member and the crystal-rich tuff member. Thin-section data represented by circles. Error bars show average $\pm 2\sigma$ precision.

which are plotted on a ternary diagram (fig. 23). Pyroxenes from the Joe Lott Tuff Member and crystal-rich tuff member plot in a very small compositional area within the augite field. A single exception is pyroxene from the middle of the lower unit; these pyroxene euhedra are endiopside and may be xenocrystic. Augite composition ranges from $Wo_{45}En_{45}Fs_{10}$ to $Wo_{40}En_{43}Fs_{17}$. Although variable iron content is the main cause of the compositional range, the normative wollastonite content of the pyroxenes, which is due to their Ca content, varies as much as 4 percent (table 17) and provides a method to compare variations in the same element (Ca) between coexisting minerals (pyroxene and apatite) as a function of stratigraphic position.

TABLE 12.—*Microprobe analyses of zircon from the Joe Lott Tuff Member and the crystal-rich tuff member*

[Analyses given in weight percent. Concentrations of Pr_2O_3 below detection limit (0.14 wt percent) and P_2O_5 below detection limit (0.10 wt percent). Fraction indicates number of analyses in which the element was detected out of total number of analyses. Average standard deviation (1σ) of each oxide for all samples as follows: ZrO_2±0.6, HfO_2±0.1, UO_2±0.02, Y_2O_3±0.25, La_2O_3±0.1, Ce_2O_3±0.03, SiO_2±0.13]

Sample	Description	Population	ZrO_2	HfO_2	UO_2	Y_2O_3	La_2O_3	Ce_2O_3	SiO_2	Total	Zr/Hf
M672	Crystal-rich tuff member,	Pink	65.51	1.08	0.22 $\frac{5}{10}$	1.75 $\frac{2}{10}$	0.30 $\frac{2}{10}$	0.12 $\frac{2}{10}$	32.78	101.76	53.0
	vitrophyre----------	Clear	64.60	1.01	.38 $\frac{4}{6}$	1.63 $\frac{3}{6}$	.34 $\frac{1}{6}$	.14 $\frac{2}{6}$	32.45	100.55	55.8
	Joe Lott Tuff Member										
M833	Upper unit----------	Pink	65.48	1.24	.17 $\frac{2}{8}$	<.80	<.18	<.05	32.75	99.64	46.1
		Clear	64.50	1.21	.11 $\frac{6}{10}$	.74	<.18	<.05	33.16	99.72	46.5
M832	Pink unit----------	Pink	65.03	1.10	.18 $\frac{6}{12}$	1.75 $\frac{8}{12}$	<.18	.15 $\frac{5}{12}$	33.15	101.36	51.6
		Clear	65.87	1.19	.11 $\frac{6}{10}$	<.60	.23 $\frac{2}{10}$	<.05	33.17	100.57	48.3
M831	Middle unit--top----------	Pink	65.71	1.14	.10 $\frac{1}{10}$	1.35 $\frac{2}{10}$	.23 $\frac{2}{10}$	<.05	32.20	100.73	50.3
		Clear	65.08	1.09	.11 $\frac{6}{10}$	.84 $\frac{1}{10}$	<.18	.09	32.85	100.06	51.3
M830	Middle unit--bottom--------	Pink	65.59	1.20	.19 $\frac{2}{12}$	<.84	.27 $\frac{2}{12}$	.11 $\frac{3}{12}$	32.63	99.99	47.7
		Clear	65.00	1.17	.13 $\frac{8}{10}$	1.12	.36 $\frac{1}{10}$	<.05	33.37	101.15	48.5
M829	Lower unit--top----------	Pink	66.51	1.19	.11 $\frac{3}{11}$	1.54	<.18	.10 $\frac{1}{11}$	33.40	102.85	48.8
		Clear	64.24	1.27	.19 $\frac{8}{10}$	1.21	<.18	<.05	33.17	100.08	44.2
M828	Lower unit--middle---------	Pink	65.78	1.27	.73 $\frac{3}{10}$	1.29	.27 $\frac{1}{10}$	<.05	32.79	102.13	45.2
		Clear	65.98	1.40	.16 $\frac{4}{10}$	.43	<.18	<.05	33.00	100.97	41.2
M827	Lower unit--bottom---------	Pink	66.09	1.24	.59 $\frac{5}{10}$	1.01	<.18	.12 $\frac{1}{10}$	32.93	101.98	46.5
		Clear	65.08	1.17	.11 $\frac{6}{10}$	.90	.27 $\frac{2}{10}$	.09 $\frac{1}{10}$	32.97	100.59	48.6
M820	Lower unit--Vitrophyre-----	Pink	64.80	1.17	.15 $\frac{5}{10}$	1.11	.23 $\frac{1}{10}$	.18 $\frac{1}{10}$	32.51	100.15	48.4
		Clear	65.18	1.02	.14 $\frac{5}{8}$	.73	<.18	<.05	32.90	99.97	55.8

Ca increases in stratigraphically higher samples within both the lower and middle cooling units, has a discontinuity in trend within the lower cooling unit, as observed for other measured parameters, as well as a discontinuity between the lower and middle tuff members.

GEOTHERMOMETRY

Several whole-rock and coexisting-mineral geothermometers were used to estimate pre-eruption thermal gradients and to correlate thermal variations with chemical variations. The only technique that seemed to provide geologically reasonable results was based on whole-rock data. The vitrophyre of the Joe Lott Tuff Member contains only about 1 percent crystals and thus represents a quenched liquid with a composition close to the liquidus. This, combined with the low CaO content and the high differentiation index (Thornton and Tuttle, 1960), suggests that, with some assumptions, magmatic compositional evolution can be modeled from whole-rock data and the experimental system $NaAlSi_3O_8$–$KAlSi_3O_8$–SiO_2–H_2O. A fluid pressure of 1 kb is considered reasonable as a first approximation of pressure conditions within the Mount Belknap magma chamber.

Figure 25 shows the projected liquidus surface for the water-saturated $NaAlSi_3O_8$–$KAlSi_3O_8$–SiO_2 system at 1-kb confining pressure. The boundary curve *wqms* separates the quartz field from the feldspar field, and *m* is the isobaric minimum. Isotherms show the configuration of the liquidus surface. The normative salic constituents in the samples from the Joe Lott Tuff Member and the crystal-rich tuff member are plotted on figure 25. Most of the samples cluster near the thermal trough with the exception of the crystal-rich tuff member (M672) and the pink unit (M832). The basal vitrophyre of the Joe Lott Tuff Member (M820) has a bulk compo-

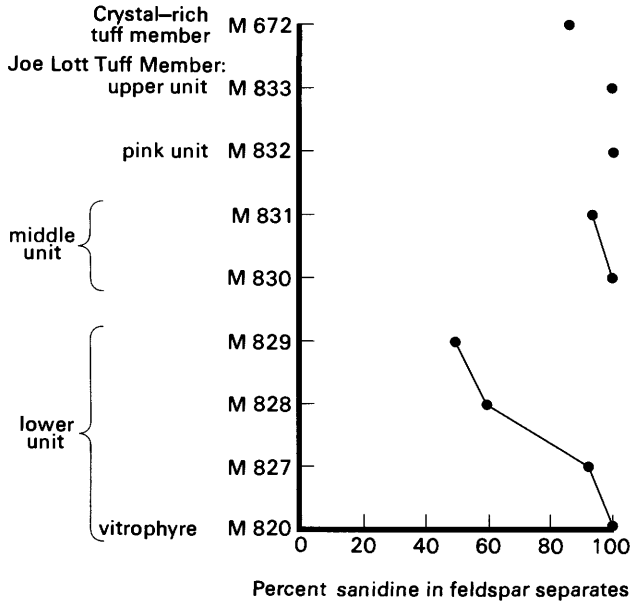

FIGURE 17.—Percentage abundance of sanidine in feldspar separates from the Joe Lott Tuff Member and the crystal-rich tuff member.

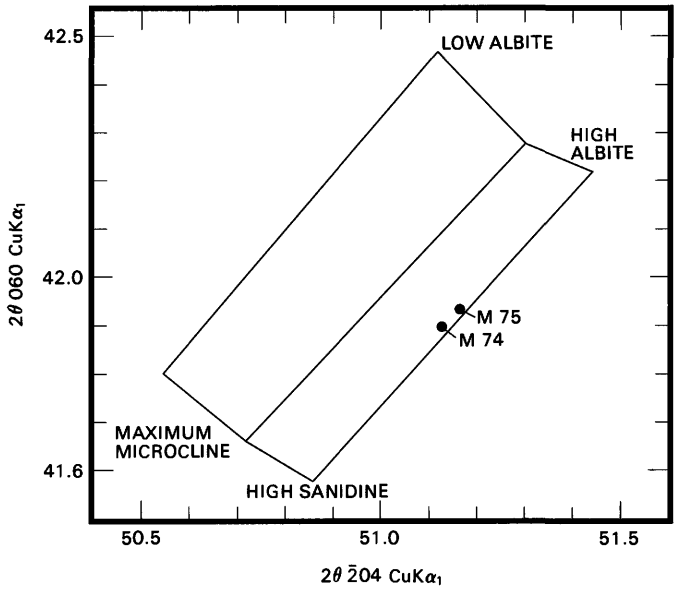

FIGURE 18.—Structural states of feldspars from the crystal- rich tuff member, based on X-ray diffraction measurements. Positions of end-member feldspars are those defined by Wright (1968).

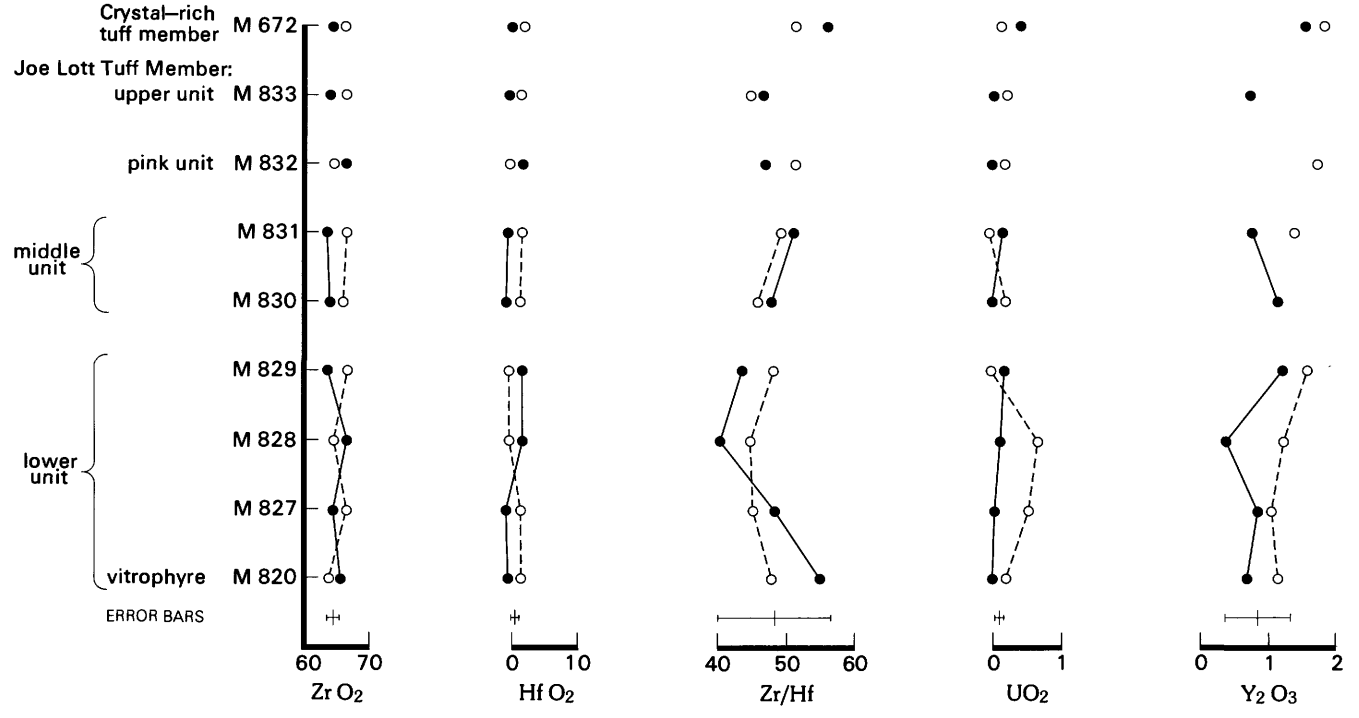

FIGURE 19.—Compositions of clear (·) and pink (○) zircons from the Joe Lott Tuff Member and the crystal-rich tuff member. Oxide abundances are in weight percent. Y_2O_3 not detected in all samples. Error bars show average $\pm 2\sigma$ precision.

sition that lies in the thermal trough and is closest to the minimum.

The temperatures of formation obtained from the $NaAlSi_3O_8$–$KAlSi_3O_8$–SiO_2–H_2O ternary diagram are shown in table 18. These temperatures systematically increase from the basal vitrophyre through the top of the lower cooling unit as successively deeper levels of the magma chamber were tapped. The anomalously high temperature for the pink unit (M832) might reflect alkali removal during postemplacement alteration

TABLE 13.—*Microprobe analyses of apatite from the Joe Lott Tuff Member and the crystal-rich tuff member*

[Analyses given in weight percent. Fraction following value indicates number of analyses in which the element was detected out of total number of analyses. Average standard deviation (1σ) of each element and oxide for all samples as follows: Cl±0.02, F±0.15, P_2O_5±0.26, CaO±0.13, Nd_2O_3±0.04, Pr_2O_3±0.11, Ce_2O_3±0.08, Y_2O_3±0.03, Le_2O_3±0.03, MgO±0.02, MnO±0.01]±

Sample	Description	Cl	F	P_2O_5	CaO	Nd_2O_3	Pr_2O_3	Ce_2O_3	Y_2O_3	La_2O_3	MgO	MnO	Total
M672	Crystal-rich tuff member,												
	vitrophyre----------	0.17	2.90 9/11	36.53	53.56	0.34	0.35 3/11	0.71	0.15 1/11	0.31 9/11	0.22	0.15	95.39
	Joe Lott Tuff Member												
M833	Upper unit----------	.11 3/8	3.16	38.37	55.30	.40 6/8	.55 1/8	.62 6/8	.15 3/8	.22	.17	.09 3/8	99.14
M832	Pink unit----------	.32 8/10	3.07	38.53	55.65	.26	<.25	.53	<.06	.20	.15	.09 2/10	98.80
M831	Middle unit--top----------	.15 5/10	3.02	38.65	53.65	.29 9/10	<.25	.51 9/10	<.06	.26 6/10	.31 6/10	.19	97.03
M830	Middle unit--bottom----------	.14 5/10	3.76	38.47	52.84	.31 6/10	<.25	.45 7/10	<.06	.16 8/10	.28 9/10	.13	96.54
M829	Lower unit--top----------	.22 6/10	2.90	39.00	53.02	.24	<.25	.65 9/10	<.06	.23 8/10	.17	.10	96.53
M828	Lower unit--middle----------	.10 6/10	3.40	38.26	52.36	.22	.50 1/10	.56 9/10	.19 1/10	.18 9/10	.23 9/10	.24 8/10	96.24
M827	Lower unit--bottom----------	.12 4/10	3.62	38.06	53.40	.27	.39 2/10	.64 9/10	<.06	.24	.15 9/10	.09 6/10	96.98
M820	Lower unit--vitrophyre--------	.39 6/10	3.15	37.40	54.61	.24	.50 1/10	.50	<.06	.24 9/10	.16 9/10	<.02	97.19

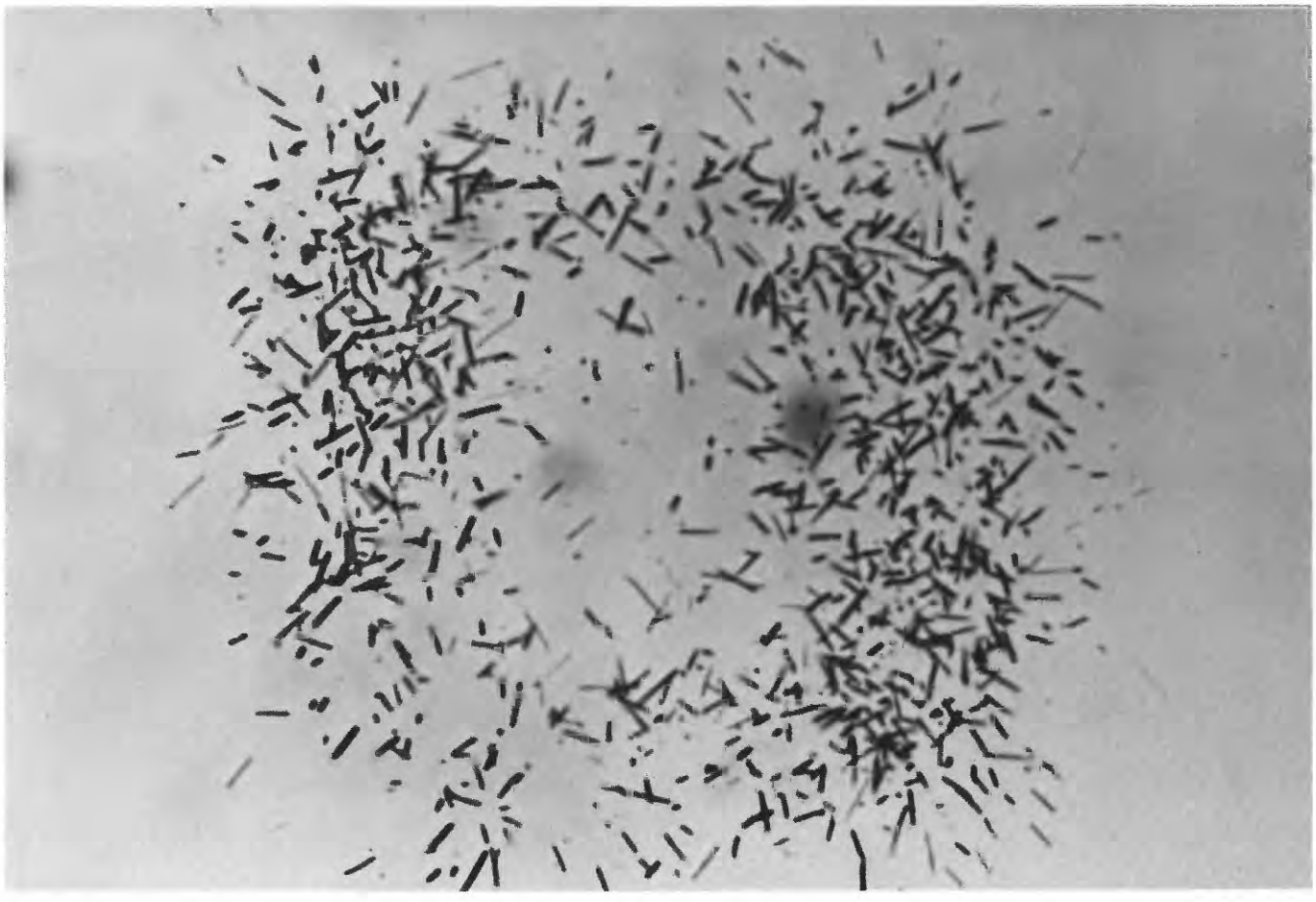

FIGURE 20.—The U distribution in pink zircon from the Joe Lott Tuff Member, determined by fission-track radiography of a polished grain mount. A high density of induced fission events at the grain margin indicates a high concentration of U toward the margin relative to the grain interior. View is 0.6 by 1.0 mm.

(Scott, 1971), which would be consistent with the relatively greater permeability of this unit. The value for sample M829 is suspect owing to the loss of Na as indicated in table 5.

When applied to the Joe Lott Tuff Member, coexisting-mineral geothermometers gave inconsistent and probably unreliable results. The postemplacement oxidation of the Fe-Ti oxide minerals in the Joe Lott Tuff Member precluded application of the Fe-Ti oxide geothermometer of Buddington and Lindsley (1964). Sanidine and plagioclase compositions from microprobe analysis of feldspar separates and of feldspar phenocrysts in thin sections were modeled on the data of Seck (1971), Stormer (1975), Brown and Parsons (1981), and Haselton and others (1983). The two-feldspar geothermometers rely on equilibrium partitioning of albite component between coexisting plagioclase and alkali feldspar. In every case it appears that the plagioclase had selectively lost K, probably by subsolidus alkali-exchange with Na.

DURATION OF ERUPTIVE SEQUENCE

The Joe Lott Tuff Member and the crystal-rich tuff member were erupted 19.2 Ma within the $\pm 2\sigma$ analytical uncertainty of ± 0.4 Ma as discussed in the section on geochronology. Within this time period, the lower, middle, and upper units of the outflow facies (Joe Lott Tuff Member) each appear to have been erupted in a more or less continuous sequence as shown by the lack of cooling breaks within them. The eruption of each may have been a matter of days, or weeks, for each unit.

Longer periods of time are represented by the intervals between the units where distinct cooling breaks are present in the outflow section; the Blue Lake Rhyolite and Mount Baldy Rhyolite Members were extruded during two of these intervals (table 1). After the Blue Lake Rhyolite Member was extruded, it had enough time to cool so that the overlying base of the intracaldera middle tuff member (fig. 2, table 1) was

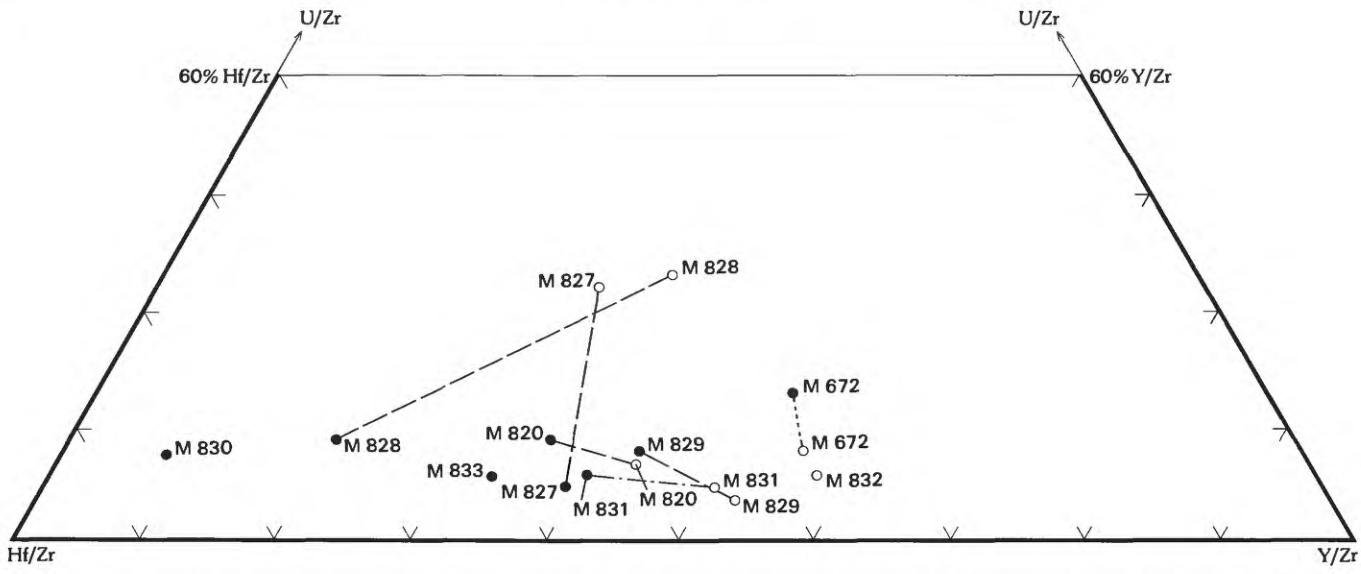

FIGURE 21.—Ternary plot of normalized U/Zr, Y/Zr, and Hf/Zr ratios in clear (·) and pink (○) zircons of the Joe Lott Tuff Member and the crystal-rich tuff member. No data point where Y below detection limit. Tie lines drawn between coexisting clear and pink zircon are as follows:

crystal-rich tuff member, vitrophyre (M672)—short dashes
Joe Lott Tuff Member
Middle cooling unit (M831)—dash, dot, dash
Lower cooling unit (M827-M829) and basal vitrophyre (M820)—long dashes

chilled in the vicinity of Mount Belknap, as shown by localized black-glass fiamme. Furthermore, sufficient time elapsed after the Blue Lake Rhyolite Member was erupted for the source magma chamber to restratify before the succeeding middle tuff member was erupted. However, in the outflow facies at the east end of Clear Creek Canyon, the top of the lower unit of the Joe Lott Tuff Member—although poorly welded—does not exhibit significant signs of erosion and channeling. Therefore, the time interval between the two ash-flow eruptions probably was several years at least, by analogy to Mt. St. Helens.

The time interval between the eruptions forming the middle and upper units was probably longer and encompassed the eruption of the Mount Baldy Rhyolite Member within the caldera, the erosional stripping of any unwelded top from the middle unit at Clear Creek, and the eruption and accumulation of the pink unit. The longer time interval may reflect a loss of eruptive energy in that more time was needed collect sufficient volatiles for further pyroclastic eruptions. The interval was probably on the order of tens of years.

The time interval between the eruption of the crystal-rich member and the Joe Lott Tuff Member was apparently significantly longer than the time it took for the Joe Lott Tuff Member to accumulate. During the interim, the Red Hills Tuff Member was erupted from its source area 14 km northeast of the Mount Belknap caldera (fig. 1). The Red Hills Tuff Member was deposited directly on the nonreworked, yet poorly welded top of the Joe Lott Tuff Member near the Red Hills caldera; again, the pristine nature of the erosionally vulnerable top indicates that not much time passed between eruption of the Joe Lott Tuff and Red Hills Tuff Members. However, a significant amount of time elapsed between eruption of the Red Hills Tuff Member and the overlying crystal-rich tuff member from the Mount Belknap caldera. The Red Hills Tuff Member was deeply eroded, and cut by channels that radiated outward to the east and south from the topographically high Mount Belknap caldera. The crystal-rich member includes a sequence of ash flows that fills these channels and unconformably overlies the Red Hills Tuff Member, Joe Lott Tuff Member, and Mount Baldy Rhyolite Member around the Mount Belknap caldera. Thus, the time interval between the eruptions of the Joe Lott Tuff Member and the crystal-rich tuff member may easily have been thousands or tens of thousands of years or more.

COMPOSITIONAL VARIATIONS IN THE JOE LOTT TUFF MEMBER

A common magmatic source for the various ash-flow units that compose the Joe Lott Tuff Member is strongly indicated by the gross chemical homogeneity

TABLE 14.—*Microprobe REE analyses of allanite from the basal vitrophyre of the Joe Lott Tuff Member*

[Analyses given in weight percent. The following elements and oxides are below sensitivity-detection limits shown in parentheses: Sm_2O_3 (0.23), Tb_2O_3 (0.16), Dy_2O_3 (0.16), Ho_2O_3 (0.29), Er_2O_3 (0.19), Tm_2O_3 (0.23), Yb_2O_3 (0.23), Lu_2O_3 (0.26)]

	Grain				
	1	4	11	13	15
Y_2O_3	.58	.30	--	.36	--
La_2O_3	7.98	8.58	9.00	7.92	7.47
Ce_2O_3	13.19	14.11	13.61	13.81	13.47
Pr_2O_3	1.08	.85	.81	1.09	1.23
Nd_2O_3	1.05	2.04	1.01	2.41	2.49
Eu_2O_3	.06	.08	.18	.19	.16
Gd_2O_3	.82	.81	.71	.76	.79

of the member. Most of the major and trace elements in the whole-rock samples do not vary significantly beyond the estimated limits of analytical precision (figs. 9 and 11), and the range of element abundances in the four samples from the lower cooling unit generally encompasses the range of concentrations measured for the entire member. This degree of homogeneity is particularly striking, considering the extent to which most of the samples are devitrified and the potential for low-temperature postemplacement alteration in these tuffs of early Miocene age.

In detail, however, several elements do exhibit analytically significant variations within and between cooling units, but interpretation of these variations is equivocal if the elements in question are relatively susceptible to postemplacement redistribution. Thus, strongest emphasis is placed on those trace elements that are geochemically least mobile during high-temperature devitrification, hydration, and alteration.

On the assumption that the fine-grained groundmass is more susceptible to alteration than are the phenocryst phases, any compositional variation in phenocryst phases is considered more reliable than whole-rock variations as an indicator of magmatic differences. Perhaps the most convincing case for differences in magmatic composition is one that documents stratigraphically coincident compositional discontinuities in several coexisting phenocryst phases and in whole rocks (Pallister and Knight, 1981). In this study, limited phenocryst and whole-rock data make the best case for a compositional discontinuity within the lower cooling unit and for another between the lower and middle cooling units. Key observations include the Or content of sanidine (fig. 15), the ratio of sanidine to total feldspar (fig. 17), and the whole-rock abundance of SiO_2, K_2O, CaO (fig. 9), and relatively immobile trace elements such as REE, Co, Cr, Sc, and Y (fig. 11). In addition, a small but systematic increase in phenocryst content upward in the lower cooling unit (table 4) suggests progressive tapping into more crystallized, deeper levels in the magma chamber. The restriction of allanite and chevkinite to the basal vitrophyre shows that the sampled part of the magma body was zoned, at least with respect to volatiles or temperature, even if only trivially so in bulk composition.

Enrichment of REE and some other elements at the top of the magma chamber is indicated by whole-rock analyses of the four samples (M820 and M827–M829) from the vertical section in Clear Creek Canyon through the lower cooling unit. REE enrichment may have a mineralogical expression with the appearance of allanite and chevkinite. There is also a suggestion that the appearance of these REE-rich phases produced a complementary depletion of REE in coexisting apatite (fig. 22) and of Y in coexisting zircon (fig. 19).

FRACTIONAL CRYSTALLIZATION

The chemical homogeneity and scarcity of phenocrysts in the Joe Lott Tuff Member reflect the minor extent of magmatic crystallization; phenocryst contents are less than 3.1 percent for all samples and less than 1.0 percent for most samples (table 4). Open-system transport of phenocrysts downward through the magma seems unlikely as the phenocrysts are unzoned; furthermore, relatively large or dense phenocrysts occur at

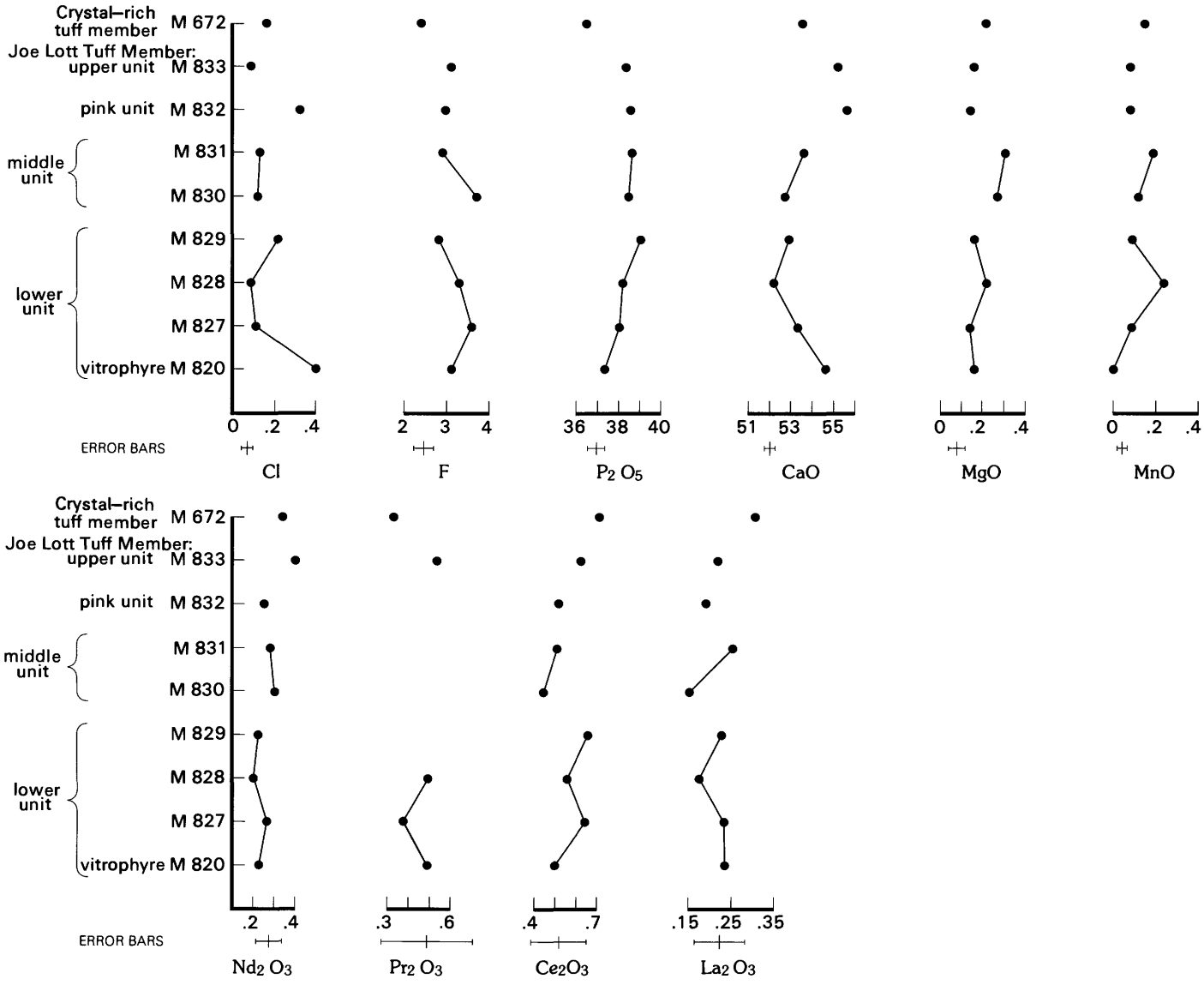

FIGURE 22.—Compositions of apatites from the Joe Lott Tuff Member and the crystal-rich tuff member. Oxide abundances are in weight percent. Pr_2O_3 not detected in all samples. Error bars show average $\pm 2\sigma$ precision.

high levels in the magma chamber, as indicated by the presence of allanite and chevkinite and relatively large grains of pyroxene in the basal vitrophyre of the lower cooling unit, which was derived from the top of the magma chamber. The magma probably was quite viscous, as indicated by the bulbous lava flows and volcanic domes with contorted flow layers that make up the Blue Lake and Mount Baldy Rhyolite Members. Chemical evidence for any settling of relatively dense phenocrysts would be indicated by elements that are highly concentrated in phenocryst phases (Zr, Hf in zircon; Sr, Eu in feldspars; REE in zircon, allanite, and chevkinite), but these elements are not selectively enriched in the upper parts of cooling units that were derived from lower levels tapped in the magma chamber (fig. 11). The apparent 1.5- to 6-fold enrichment of some elements (Mn, Mo, U, Cs, Co, Cr, Li) in the basal vitrophyre of the lower cooling unit is grossly inconsistent with the limited degree to which the magma had crystallized. An alternative to fractional crystallization is limited *closed-system* stratification of almost entirely liquid magma in the pre-eruptive magma chamber.

THERMOGRAVITATIONAL DIFFUSION

Liquid-state fractionation of elements is an important mechanism by which high-silica (>75 wt percent SiO_2) magmas can differentiate (Shaw and others, 1976; Hildreth, 1976, 1977, 1979, 1981, 1983). Liquid-state fractionation, alternatively termed "thermogravitational

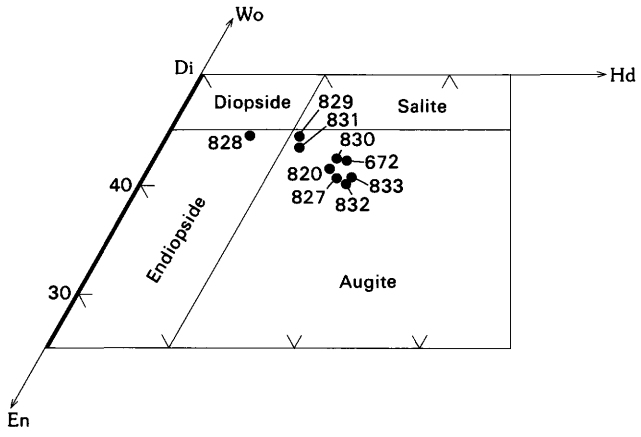

FIGURE 23.—Composition of pyroxene in the Joe Lott Tuff Member and the crystal-rich tuff member.

diffusion" (TGD), employs thermally driven, convection-aided chemical diffusion to transport and concentrate ions, volatiles, and complex molecules in a magma. According to the TGD model (fig. 26), a rising boundary layer enriched in volatile components and metal ions moves upward at the steep interface between a convecting magma body and cooler wall rocks and forms a compositionally distinct, gravitationally stable layer near the roof of the magma chamber. Element partitioning in this roof-zone magma is strongly influenced by the volatile content and the structural state (degree of polymerization) of the melt (Mahood, 1981).

Hildreth (1977) used TGD to explain compositional gradients in the Bishop Tuff that apparently could not be explained by crystal-liquid partitioning. Recent studies of the products of silicic volcanism and plutonism describe compositional gradients that are similar, but not identical, to those found in the Bishop Tuff (Smith, 1979; Mahood, 1981; Bacon, 1981; Crecraft and others, 1981; Ludington, 1981). Proponents of TGD explain that observed inconsistencies are caused by differences in the amount and relative abundance of volatile constituents that strongly affect metal-complex formation, melt polymerization, and crystal-liquid and vapor-liquid partitioning of elements (Mahood, 1981; Hildreth, 1983). Critics of TGD claim that more accurate evaluation of the effects of trace-element-rich accessory minerals can explain some compositional effects now attributed to TGD (Miller and Mittlefehldt, 1982), and that concentration gradients in the Bishop Tuff *are* consistent with a fractional crystallization process, but one that occurs at the contacts of magma and wall rock rather than in the roof-zone magma (Michael, 1983a,b; Christiansen, 1983).

Observed compositional gradients in the lower cooling unit of the Joe Lott Tuff Member indicate general

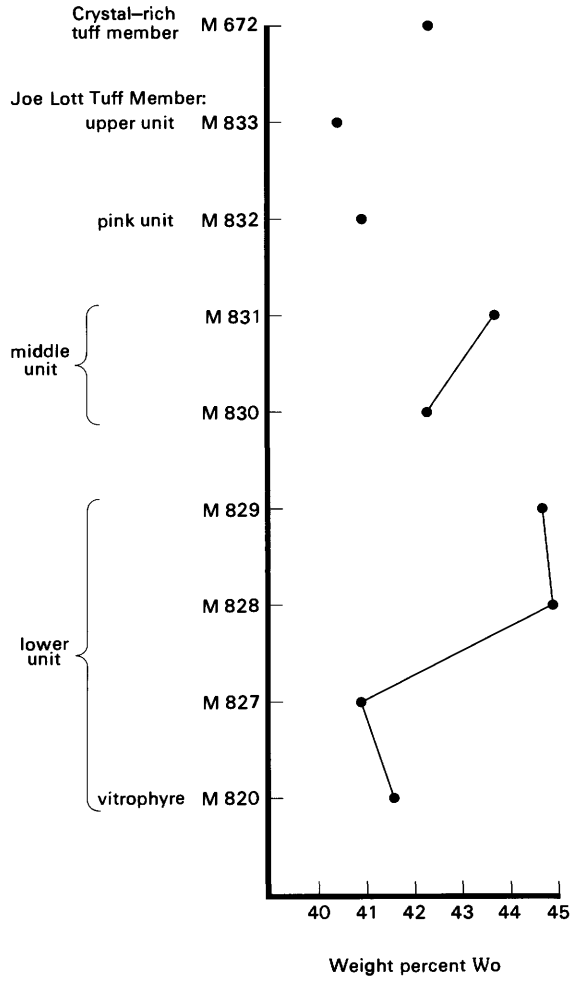

FIGURE 24.—Normative wollastonite (Wo) content (as weight percent) of pyroxenes in the Joe Lott Tuff Member and crystal- rich tuff member as a function of stratigraphy.

roofward enrichment of most trace elements, which contrasts with the more complex pattern of enrichments and depletions observed in the Bishop Tuff (fig. 13). In particular, TGD was invoked by Hildreth to explain antithetic behavior within groups of geochemically similar elements such as the REE and transition metals, but such behavior is not apparent in the Joe Lott.

The Joe Lott Tuff Member would be expected to have less compositional zoning than the Bishop Tuff. Not only is the Joe Lott a significantly smaller volume, but probably more important, the range of pre-eruptive temperatures in the Joe Lott (750–770 °C) is significantly less than in the Bishop (720–790 °C).

Roofward enrichment of volatiles within the lower cooling unit is indicated by the apparent roofward decrease in phenocryst content, by a higher Cl content of early-erupted apatite (fig. 22), and by the occurrence of hydrous silicates such as allanite exclusively in the

TABLE 15.—*Microprobe analyses of chevkinite from the basal vitrophyre of the Joe Lott Tuff Member*

[Analyses given in weight percent. The following oxides are below sensitivity-detection limits shown in parentheses: Na_2O (0.05), P_2O_5 (0.10), MnO (0.02), Tb_2O_3 (0.16), Dy_2O_3 (0.16), Ho_2O_3 (0.29), Er_2O_3 (0.19), Tm_2O_3 (0.23), Yb_2O_3 (0.23), Lu_2O_3 (0.26), UO_2 (0.50)]

	Grain								
	3	5	6	7	9	12	14	16	17
SiO_2----	18.56	18.43	17.52	17.08	18.21	16.93	17.07	18.88	17.32
Al_2O_3---	2.51	2.60	.86	.84	2.67	.78	.89	2.81	2.54
TiO_2----	17.39	19.92	21.29	21.41	21.59	22.23	20.49	22.45	20.98
FeO-----	4.96	4.61	6.49	6.48	4.85	6.03	6.02	5.05	4.74
MgO-----	.91	1.07	.81	.80	.88	.83	.93	.62	.97
CaO-----	5.18	4.02	3.80	3.67	5.08	3.64	4.02	5.20	5.52
Y_2O_3----	.58	.62	.74	.34	.32	.60	.55	.60	.65
La_2O_3---	10.70	11.98	10.69	10.88	11.36	11.00	10.06	11.68	10.85
Ce_2O_3---	22.37	24.72	23.15	22.57	22.84	23.08	22.16	22.60	21.48
Pr_2O_3---	2.07	2.12	2.11	2.01	2.15	2.07	2.36	2.01	1.70
Nd_2O_3---	4.84	5.95	6.05	5.63	4.48	3.97	5.42	5.78	5.00
Sm_2O_3---	.86	.60	1.03	.42	.52	.38	.89	.43	.44
Eu_2O_3---	.27	.39	.46	.21	.25	.47	.28	.41	.27
Gd_2O_3---	1.49	1.71	2.06	1.83	1.24	2.00	1.72	1.69	1.57
ThO_2----	4.81	2.18	5.45	7.23	3.21	6.40	8.39	2.95	4.55
F-------	.44	.59	--	--	.48	--	--	--	.62
	97.94	101.51			100.13				99.20
O=F-----	.18	.25			.20				.26
Total	98.12	101.76	102.51	101.40	100.33	100.41	101.25	103.16	99.46

early-erupted magma. However, the directly measured enrichment of H_2O in the early-erupted basal vitrophyre (fig. 13) is a result of preferential secondary hydration of the constituent glass and is discounted. Although the Joe Lott magma probably was enriched in volatiles, the effect of these volatiles on the compositional gradients of individual elements is uncertain and unpredictable. Qualitative arguments based on a limited understanding of volatile transport and melt structural effects are possible within the framework of TGD, but remain unconvincing unless supported by independent evidence. In the case of the Joe Lott Tuff Member, compositional variations of most elements are analytically insignificant or involve elements that are subject to redistribution by postmagmatic processes. Thus it is difficult to attribute the spectrum of observed compositional variations solely to TGD.

POSTMAGMATIC MODIFICATIONS

Apparent enrichments of Mn, Mo, U, Cs, and Li in the basal vitrophyre of the Joe Lott Tuff Member (fig. 13) are too large to explain by fractional crystallization. Volatile transport or liquid-state diffusion in the roof-zone magma are possible explanations, but are difficult to distinguish from possible effects of postemplacement alteration. This suite of elements is typically depleted in devitrified rhyolite compared to coexisting obsidian

TABLE 16.—*Microprobe analyses of pyroxene from the Joe Lott Tuff Member and the crystal-rich tuff member*
[Analyses given in weight percent. K_2O and Cr_2O_3 are below detection unit of 0.01 and 0.02 wt percent, respectively]

	M820		M827		M828		M829		M830		M831		M832		M833		M672	
SiO_2---	50.95		48.16		52.36		49.88		52.02		51.17		52.13		51.76		49.08	
Al_2O_3--	2.36		4.86		2.45		3.66		1.42		4.42		3.07		2.15		2.53	
TiO_2---	.88		1.30		.33		.51		.40		1.16		.94		.98		.77	
FeO----	10.36		8.51		4.25		6.42		8.44		7.04		9.59		10.10		8.04	
MnO----	.45		.24		.09		.18		1.28		.18		.16		.33		.99	
MgO----	15.54		15.52		17.33		16.37		14.91		15.91		15.07		15.44		14.98	
CaO----	19.52		20.56		21.77		21.67		21.05		20.99		20.08		19.87		21.08	
Na_2O---	.53		.71		.89		.40		.88		.68		.81		.61		.92	
Total--	100.59		99.86		99.47		99.09		100.40		101.55		101.85		101.24		98.39	
Formulae calculated on basis of 6 oxygens																		
Si-----	1.899	2.000	1.805	2.000	1.921	2.000	1.863	2.000	1.941	2.000	1.858	2.000	1.905	2.000	1.912	2.000	1.874	2.000
Al-----	.103		.215		.106		.162		.062		.167		.132		.094		.114	
Ti-----	.025		.037		.009		.014		.012		.032		.026		.028		.022	
Fe-----	.323		.267		.131		.201		.264		.214		.293		.312		.257	
Mn-----	.014	2.046	.008	2.078	.003	2.037	.006	2.055	.040	2.051	.006	2.004	.005	2.026	.010	2.036	.032	2.083
Mg-----	.864		.868		.948		.912		.829		.862		.821		.850		.853	
Ca-----	.780		.826		.856		.868		.839		.817		.787		.787		.863	
Na-----	.038		.052		.063		.029		.064		.048		.057		.043		.068	

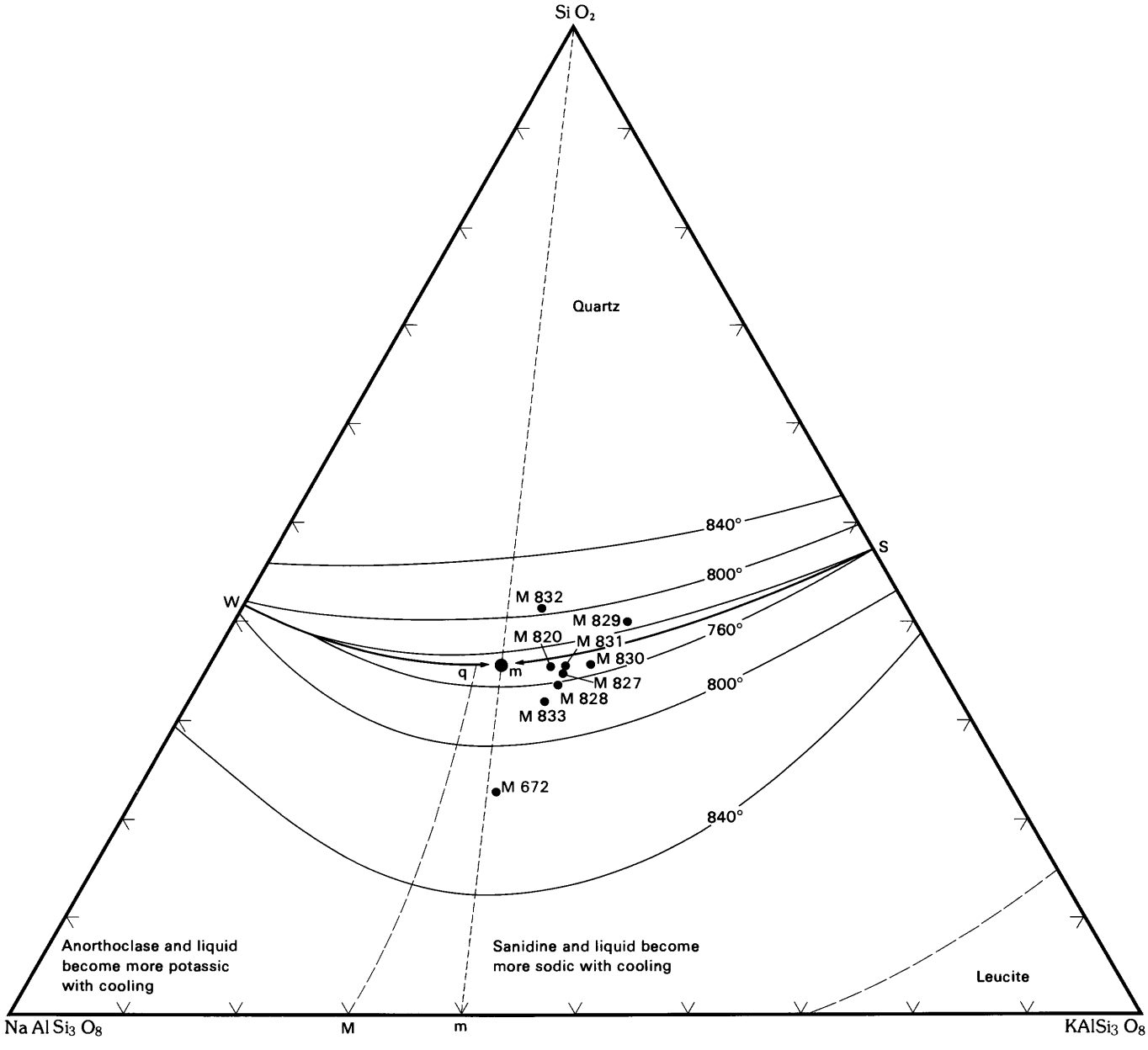

FIGURE 25.—Normative salic compositions from the Joe Lott Tuff Member and the crystal-rich tuff member plotted on the liquidus surface for H_2O-saturated liquids at 1-kb confining pressure in the system $NaAlSi_3O_8$-$KAlSi_3O_8$-SiO_2-H_2O (Tuttle and Bowen, 1958; Carmichael and others, 1974). Temperature in degrees Celsius.

(see Zielinski and others, 1977, for a review). Thus, apparent enrichment of these elements in the basal vitrophyre (M820) may result from selective removal of elements from overlying devitrified parts of the cooling unit during cooling and subsequent alteration. Other variations possibly related to postmagmatic alteration include the greater abundance of Mn, Mo, U, Cs, Sr, and F in the relatively vitric pink unit as contrasted with smaller contents in devitrified units of the Joe Lott Tuff Member. Similar comparisons indicate that alkalies, alkaline-earths, and halogens are subject to redistribution during devitrification, glass hydration, and alteration (Friedman and Harris, 1961; Orville, 1963; Lipman, 1965; Lipman and others, 1969; Noble, 1965, 1967; Noble and others, 1967; Lofgren, 1970; Scott, 1971; Zielinski and others, 1977). Whole-rock abundances of affected trace elements are expected to vary most as a result of postemplacement modifications, but Na and K contents of whole rocks and phenocrysts also appear to be affected. For example, demonstrated subsolidus redistribution of K_2O in plagioclase makes this mineral unusable as a geothermometer in the Joe Lott.

TABLE 17.—*Calculated abundance of pyroxene end member in pyroxenes from the Joe Lott Tuff Member and the crystal-rich tuff member*

Sample	Description	X_{Wo}	X_{En}	X_{Fs}
M672	Crystal-rich tuff member, vitrophyre	42.30	42.52	15.18
	Joe Lott Tuff Member			
M833	Upper unit----------	40.41	43.00	16.59
M832	Pink unit----------	40.96	43.45	15.59
M831	Middle unit--top----------	43.73	45.31	10.96
M830	Middle unit--bottom----------	42.26	42.90	14.84
M829	Lower unit--top----------	44.72	44.93	10.35
M828	Lower unit--middle----------	44.91	48.75	6.34
M827	Lower unit--bottom----------	40.86	43.80	15.34
M820	Lower unit--vitrophyre----------	41.58	43.96	14.46

CONTAMINATION EFFECTS

Lithic fragments with long dimensions greater than about 2 mm were hand picked from coarsely crushed samples prior to final grinding and analysis. An upper limit for the modal abundance of remaining small lithic fragments in each analyzed sample was obtained from thin-section observations; these showed that less than 1 percent of the grains are lithic fragments smaller than 2 mm. This small abundance and the fact that most foreign lithic fragments are rhyolite suggest that the compositional effect of contamination is minimal. Contamination effects are best illustrated by trace elements because of potentially large compositional contrasts between host and contaminant. For example, the Three Creeks Tuff Member of the Bullion Canyon Volcanics, which directly underlies the Joe Lott Tuff Member in the sampling area, contains more than 6 times as much Sc, 10 times as much Ba and Sr, and more than 20 times as much Co and Cr as average Joe Lott (C. G. Cunningham, unpublished data). The apparent enrichments of Ba, Co, Cr, and Sc in the basal vitrophyre can be modeled by incorporation of approximately 1 wt percent lithic fragments of Three Creeks composition. Sr is not similarly enriched in basal vitrophyre but is subject to postmagmatic redistribution. Enrichments of U, Mo, Mn, Cs, and Li in the basal vitrophyre are too large and in the wrong direction to be explained by contamination from the underlying, more mafic Bullion Canyon Volcanics.

Two coexisting populations of compositionally distinct zircons—one clear and homogeneous and the other pink and commonly with U-rich rims—throughout the Joe Lott Tuff Member (fig. 21) suggest an efficient mixing process if either type of zircon was derived from a contaminating source or by mixing of partly crystallized, different magmas. However, as noted earlier, extensive vertical transport of phenocrysts within the shallow pre-eruptive magma of the Joe Lott is not supported by total phenocryst abundances or by the chemistry of phenocrysts and whole rocks. Perhaps magma convection at depth mixed zircons of different provenance prior to crystallization of the other phenocrysts. Slight differences in zircon chemistry may distinguish zircons that crystallize in response to wall-rock interactions from those that crystallize in the main magma body.

The above observations suggest that incorporation of small quantities of foreign lithic fragments into the Joe Lott magma had little effect on whole-rock compositions. The most likely exception is the basal vitrophyre, and the most affected elements are Co, Cr, Ba, and Sc. Some wall-rock interaction at depth is suggested by the homogeneous distribution and the contrasting chemistry of two populations of coexisting zircons.

SUMMARY

Of the measured parameters, the REE are considered to be the most reliable indicators of magmatically caused compositional variations in the Joe Lott Tuff Member. Compositional trends and discontinuities identified on the basis of REE abundances include (1) slight (5 to 15 percent) roofward enrichment in the lower cooling unit and (2) compositional discontinuities in the lower cooling unit and between the lower and middle cooling units. Element enrichments in the lower cooling

TABLE 18.—*Estimated temperatures of crystallization of the Joe Lott Tuff Member and the crystal-rich tuff member*

[From whole-rock normative salic compositions plotted (fig. 25) on the liquidus surface for H_2O-saturated liquids at 1 kb in the system $NaAlSi_3O_8$-$KAlSi_3O_8$-SiO_2 (Tuttle and Bowen, 1958; Carmichael and others, 1974)]

Sample	Description	Temperature in °C
M672	Crystal-rich tuff member, vitrophyre--	810
	Joe Lott Tuff Member	
M833	Upper unit----------	770
M832	Pink unit----------	800
M831	Middle unit--top----------	750
M830	Middle unit--bottom----------	760
M829	Lower unit--top----------	770
M828	Lower unit--middle----------	760
M827	Lower unit--bottom----------	760
M820	Lower unit--vitrophyre----------	750

unit that greatly exceed those of the REE cannot be unambiguously assigned to either magmatic or post-magmatic causes. Apparent discontinuities in whole-rock or phenocryst compositions are tentatively assigned to magmatic causes to the extent that they are stratigraphically coincident with discontinuities in REE abundances. Measurements showing discontinuities that best meet this criterion include the composition and relative abundance of sanidine and the whole-rock abundances of SiO_2, K_2O, CaO, Mn, Sc, Co, Cr, and Y.

The small roofward enrichment of REE in the lower cooling unit is qualitatively consistent with a fractional crystallization mechanism, but the lack of increased fractionation of Eu from other REE (an indication that early feldspar segregation was minor) suggests that if significant crystal-melt segregation occurred, it happened before the shallow emplacement of magma and crystallization of the observed feldspar-rich phenocryst assemblages. A similar conclusion is reached from observations of the composition and abundance of phenocrysts at different stratigraphic levels. An alternative mechanism that calls for crystal-melt segregation at depth involves variable fractional crystallization at contacts between magma and wall rock. Crystals accumulate at contacts while less dense magma rises in the counter-flowing boundary layer to density-stratify in a shallow chamber (Michael, 1983a, b; Christiansen, 1983). Alternatively, compositional variations could be caused by liquid-state differentiation (TGD), but critical evaluation of this mechanism is hampered because of the possible effects of postemplacement alteration on the abundance of several trace elements.

Compositional discontinuities between cooling units can be accounted for by injecting new magma into the magma chamber or re-establishing compositional gradients in the magma after a partial eruption. Compositional discontinuities within single cooling units may have similar causes, but the time frame is considerably shortened to coincide with the period of eruption. In the Joe Lott Tuff Member, the compositional discontinuity within the lower cooling unit suggests a resetting of compositions to more primitive values. Variations in whole-rock SiO_2, CaO, and K_2O abundances and those of most of the trace elements are stratigraphically consistent. Variations within minerals, such as the Ab content of sanidine, Y_2O_3 content of clear zircons, and Nd_2O_3 and Ce_2O_3 contents of apatites follow the same pattern. Some other elemental abundances, such as whole-rock Fe and Mo, vary in a consistent, antithetical direction. This may indicate an injection of new, less evolved magma during evacuation of a shallow magma chamber, uneven evacuation of the chamber, or evacuation of an irregularly shaped chamber.

RELATION OF THE CRYSTAL-RICH TUFF MEMBER TO THE JOE LOTT TUFF MEMBER

Trace-element abundances in the crystal-rich tuff member are generally higher than in the Joe Lott Tuff

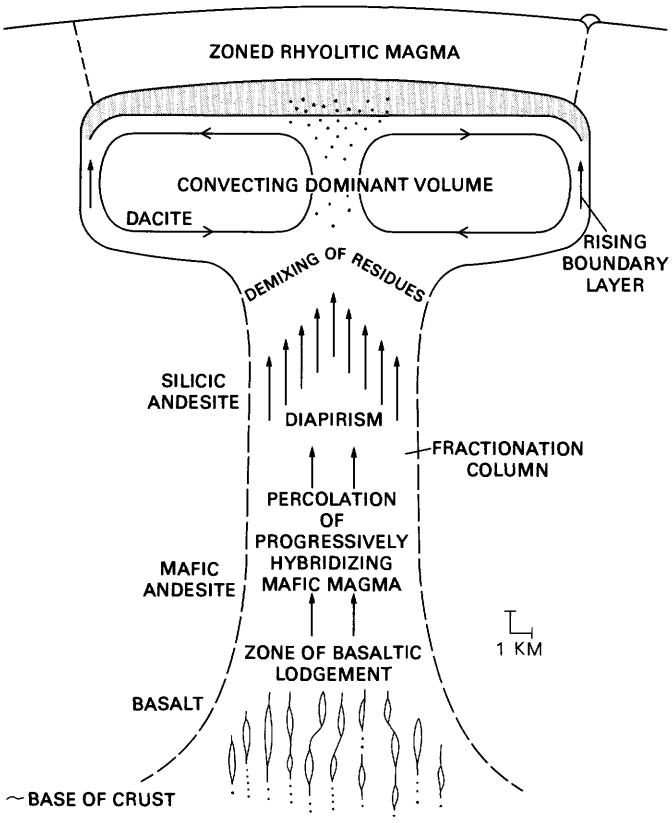

FIGURE 26.—Schematic diagram of the convection-driven thermogravitational diffusion model (modified after Hildreth, 1981).

Member, with enrichments of some elements (Ba, Sr, REE, Sc, Y, Zr, Hf) approaching, and sometimes exceeding, a factor of two (table 7, figs. 11 and 12). If the crystal-rich tuff member is to be modeled as representing the magma from which the more silicic, relatively crystal-poor Joe Lott developed, these differentiation-related depletions in the Joe Lott must be explained. If the compositional changes are to form by fractionational crystallization, the crystallizing assemblage must be able to compete effectively with coexisting melt for the depleted elements, that is, their bulk distribution coefficients must be >1. This requires major removal of phases that are sinks for the depleted elements—feldspars (Sr, Ba), zircon (Zr, Hf), mafic phases (Sc), and REE-rich accessory minerals. Quantitative modeling was not attempted because of large uncertainties in the estimates of modal abundances of accessory minerals and in the choice of appropriate mineral-liquid distribution coefficients for highly silicic magmas (Mahood, 1983). Abundances of Zr, Hf, and REE that decrease with increasing differentiation are not usually observed, except in some highly silicic (>75 wt percent SiO_2) magmas, and as discussed herein, the compatibility of such observations with fractional crystallization in a magma is the subject of some debate.

An alternative to fractional crystallization is liquid-state differentiation (TGD), which has been used to explain similar compositional trends in the Bishop Tuff, but differentiation-related depletions of *all* the REE and of Sc and Y are not observed in the Bishop Tuff (fig. 13).

A difficult problem for either model to resolve is the fact that similar (differentiation-related?) depletions of certain elements are not observed within the highly silicic compositions of the Joe Lott Tuff Member. For example, compositional trends of REE and Sc within the lower cooling unit indicate slight roofward *enrichment* (figs. 12 and 13). Based on this apparent inconsistency, our tentative conclusion is that the crystal-rich tuff member is not comagmatic with the Joe Lott Tuff Member. The two members may be products of melting of a compositionally heterogeneous source area beneath the Marysvale volcanic field. Based on chondrite-normalized REE patterns and Zr/Hf ratios, the crystal-rich tuff member has closer affinity with quartz monzonites of the Bullion Canyon Volcanics, which predate the Mount Belknap caldera (C. G. Cunningham, unpublished data). The crystal-rich tuff member may well represent a partial melt of the same source area that generated these older rocks.

REFERENCES CITED

Bacon, C. R., 1981, Pleistocene high-silica rhyolites of the Coso Volcanic Field, Inyo County, California: Journal of Geophysical Research, v. 86, no. B11, p. 10223–10241.

Best, M. G., McKee, E. H., and Damon, P. E., 1980, Space-time-composition patterns of late Cenozoic mafic volcanism, southwestern Utah and adjoining areas: American Journal of Science, v. 280, p. 1035–1050.

Brown, W. L., and Parsons, Ian, 1981, Towards a more practical two-feldspar geothermometer: Contributions to Mineralogy and Petrology, v. 76, p. 369–377.

Budding, K. E., 1982, Eruptive history, petrology, and petrogenesis of the Joe Lott Tuff Member of the Mount Belknap Volcanics, Marysvale volcanic field, west-central Utah: U.S. Geological Survey Open-File Report 82–891, 74 p.

Buddington, A. F., and Lindsley, D. H., 1964, Iron-titanium oxide minerals and synthetic equivalents: Journal of Petrology, v. 5, no. 2, p. 310–357.

Carmichael, I. E., Turner, F. J., and Verhoogen, John, 1974, Igneous petrology: New York, McGraw-Hill Book Company, 739 p.

Christiansen, E. C., 1983, The Bishop tuff revisited: Compositional zonation in double-diffusive fractional crystallization: Geological Society of America Abstracts with Programs, v. 15, no. 5, p. 390.

Crecraft, H. R., Nash, W. P., and Evans, S. H., Jr., 1981, Late Cenozoic volcanism at Twin Peaks, Utah: Geology and petrology: Journal of Geophysical Research, v. 86, no. B11, p. 10303–10320.

Cunningham, C. G., Ludwig, K. R., Naeser, C. W., Weiland, E. K., Mehnert, H. H., Steven, T. A., and Rasmussen, J. D., 1982, Geochronology of hydrothermal uranium deposits and associated igneous rocks in the eastern source area of the Mount Belknap Volcanics, Marysvale, Utah: Economic Geology, v. 77, no. 2, p. 444–454.

Cunningham, C. G., Rye, R. O., Steven, T. A., and Mehnert, H. H., 1984, Origins and exploration significance of replacement and vein-type alunite deposits in the Marysvale volcanic field, west-central Utah: Economic Geology, v. 79, no. 1, p. 50–71.

Cunningham, C. G., and Steven, T. A., 1979, Mount Belknap and Red Hills calderas and associated rocks, Marysvale volcanic field, west-central Utah: U.S. Geological Survey Bulletin 1468, 34 p.

Cunningham, C. G., Steven, T. A., Campbell, D. L., Naeser, C. W., Pitkin, J. A., and Duval, J. S., 1984, Multiple episodes of igneous activity, mineralization, and alteration in the western Tushar Mountains, Utah, Chapter A *in* Steven, T. A., ed., Igneous activity and related ore deposits in the western and southern Tushar Mountains, Marysvale volcanic field, west-central Utah: U.S. Geological Survey Professional Paper 1299–A, p. 1–21.

Cunningham, C. G., Steven, T. A., Rowley, P. D., Glassgold, L. B., and Anderson, J. J., 1983, Geologic map of the Tushar Mountains and adjoining areas, Marysvale volcanic field, Utah: U.S. Geological Survey Miscellaneous Investigations Series Map I–1430–A, scale 1:50,000.

———1984, Map of argillic and advanced argillic alteration and principal hydrothermal quartz and alunite veins in the Tushar Mountains and adjoining areas, Marysvale volcanic field, Utah: U.S. Geological Survey Miscellaneous Investigations Series Map I–1430–B, scale 1:50,000.

Dalrymple, G. B., and Lanphere, M. A., 1969, Potassium-argon dating: San Francisco, W. M. Freeman and Company, 258 p.

Deer, W. A., Howie, R. A., and Zussman, J., 1963, Framework silicates, v. 4 *of* Rock-forming minerals: London, Longmans, Green and Co., Ltd., 435 p.

Effinroff, I., 1972, The chemical and morphological variations of zircons from the Boulder batholith, Montana: Cincinnati, Ohio, University of Cincinnati, unpublished Ph. D. thesis, 136 p.

Friedman, I., and Harris, J., 1961, Fluorine during hydration of rhyolitic glass: U.S. Geological Survey Professional Paper 424–C, p. C304–C305.

Gordon, G. E., Randel, K., Goles, G. G., Corliss, J. B., Benson, M. H., and Oxley, S., 1969, Instrumental activation analysis of standard rocks with high resolution X-ray detectors: Geochimica et Cosmochimica Acta, v. 32, p. 369–396.

Haselton, H. T., Jr., Horis, G. L., Hemingway, B. S., and Robie, R. A., 1983, Calorimetric investigation of the excess entropy of mixing in albite-sanidine solid solutions: Lack of evidence for Na, K short-range order and implications for two-feldspar thermometry: American Mineralogist, v. 68, p. 398–413.

Hildreth, E. W., 1977, The magma chamber of the Bishop Tuff: Gradients in temperature, pressure, and composition: Berkeley, California, University of California, unpublished Ph. D. thesis, 328 p.

Hildreth, W., 1976, The Bishop Tuff: Compositional zonation in a silicic magma chamber without crystal settling [abs.]: Geological Society of America Abstracts with Programs, v. 8, p. 918.

Hildreth, W., 1979, The Bishop Tuff: Evidence for the origin of compositional zonation in silicic magma chambers: Geological Society of America Special Paper 180, p. 43–75.

———1981, Gradients in silicic magma chambers: Journal of Geophysical Research, v. 86, no. B11, p. 10153–10192.

———1983, Comment and reply on "Chemical differentiation of the Bishop Tuff and other high-silica magmas through crystallization processes"—Comment: Geology, v. 11, no. 10, p. 622–623.

Keith, T. E. C., Thompson, J. M., and Mays, R. E., 1983, Selective concentration of cesium in analcime during hydrothermal alteration, Yellowstone National Park, Wyoming: Geochimica et Cosmochimica Acta, v. 47, p. 795–804.

Lipman, P. W., 1965, Chemical comparison of glassy and crystalline volcanic rocks: U.S. Geological Survey Bulletin 1201–D, p. 29–39.

Lipman, P. W., Christiansen, R. L., and O'Connor, J. T., 1966, A compositionally zoned ash-flow sheet in southern Nevada: U.S. Geological Survey Professional Paper 524–F, 47 p.

Lipman, P. W., Christiansen, R. L., and Van Alstine, R. E., 1969, Retention of alkalies by calc-alkaline rhyolites during crystallization and hydration: American Mineralogist, v. 54, p. 286–291.

Lofgren, G., 1970, Experimental devitrification of rhyolite glass: Geological Society of America Bulletin, v. 81, p. 553–560.

Ludington, S., 1981, The Redskin Granite—evidence for thermogravitational diffusion in a Precambrian granite batholith: Journal of Geophysical Research, v. 86, no. B11, p. 10423–10430.

Mahood, G. A., 1981, A summary of the geology and petrology of the Sierra La Primavera, Jalisco, Mexico: Journal of Geophysical Research, v. 86, no. B11, p. 10137–10152.

———1983, Large partition coefficients for trace elements in high-silica rhyolites: Geochimica et Cosmochimica Acta, v. 47, p. 11–30.

Michael, P. J., 1983a, Chemical differentiation of the Bishop Tuff and other high-silica magmas through crystallization processes: Geology, v. 11, p. 31–34.

———1983b, Comment and reply on "Chemical differentiation of the Bishop Tuff and other high-silica magmas through crystallization processes"—Reply: Geology, v. 11, no. 10, p. 623–624.

Millard, M. T., Jr., and Keaten, B. A., 1982, Precision of uranium and thorium determination by delayed neutron counting: Journal of Radioanalytical Chemistry, v. 72, no. 1, p. 489–500.

Miller, C. F., and Mittlefehldt, D. W., 1982, Depletion of light rare-earth elements in felsic magmas: Geology, v. 10, no. 3, p. 129–133.

Noble, D. C., 1965, Ground water leaching of sodium from quickly cooled volcanic rocks: American Mineralogist, v. 50, p. 289.

———1967, Sodium, potassium and ferrous iron contents of some secondarily hydrated natural silicic glasses: American Mineralogist, v. 52, p. 280–286.

Noble, D. C., Smith, V. C., and Peck, L. C., 1967, Loss of halogens from crystallized and glassy silicic volcanic rocks: Geochimica et Cosmochimica Acta, v. 31, p. 215–233.

Orville, P. M., 1963, Alkali-ion exchange between vapor and feldspar phases: American Journal of Science, v. 261, p. 201–237.

Pallister, J. S., and Knight, R. J., 1981, Rare-earth element geochemistry of the Samail ophiolite near Ibra, Oman: Journal of Geophysical Research, v. 86, no. B4, p. 2673–2697.

Rowley, P. D., Steven, T. A., and Mehnert, H. H., 1981, Origin and structural implications of upper Miocene rhyolites in Kingston Canyon, Piute County Utah: Geological Society of America Bulletin, pt. I, v. 92, no. 8, p. 590–602.

Scott, R. B., 1971, Alkali exchange during devitrification and hydration of glasses in ignimbrite cooling units: Journal of Geology, v. 79, p. 100–110.

Seck, H. A., 1971, Alkali feldspar-liquid and alkali feldspar- liquid-vapor relationships at pressures of 5 and 10 kbar: Neues Jahrbuch für Mineralogie Abhandlungen, v. 115, no. 2, p. 140–163.

Shapiro, L., 1975, Rapid analysis of silicate, carbonate, and phosphate rocks: U.S. Geological Survey Bulletin 1401, 76 p.

Shaw, H. R., Smith, R. L., and Hildreth, W., 1976, Thermogravitational mechanisms for chemical variations in zoned magma chambers [abs.]: Geological Society of America Abstracts with Programs, v. 8, p. 1102.

Smith, R. L., 1979, Ash-flow magmatism: Geological Society of America Special Paper 180, p. 5–27.

Smith, R. L., and Bailey, R. A., 1966, The Bandelier Tuff: A study of ash-flow eruption cycles from zoned magma chambers: Bulletin Volcanologique, ser. 2, v. 29, p. 83–104.

Steven, T. A., Cunningham, C. G., and Machette, M. N., 1981, Integrated uranium systems in the Marysvale volcanic field, west-central Utah, *in* Goodell, P. C., and Waters, Aaron, C., eds., Uranium in volcanic and volcaniclastic rocks: American Association of Petroleum Geologists Studies in Geology no. 13, p. 111–122.

Steven, T. A., Cunningham, C. G., Naeser, C. W., and Mehnert, H. H., 1979, Revised stratigraphy and radiometric ages of volcanic rocks in the Marysvale area, west-central Utah: U.S. Geological Survey Bulletin 1469, 40 p.

Steven, T. A., and Morris, H. T., 1983, Geologic map of the Richfield 1°x2° quadrangle, Utah: U.S. Geological Survey Open-File Report 83–583.

Steven, T. A., Rowley, P. D., and Cunningham, C. G., 1984, Calderas of the Marysvale volcanic field, west-central Utah: Journal of Geophysical Research, v. 89, no. B10, p. 8751–8764.

Stormer, J. C., Jr., 1975, A practical two-feldspar geothermometer: American Mineralogist, v. 60, no. 7–8, p. 667–674.

Stuckless, J. S., and Van Trump, G., Jr., 1979, A revised version of graphic normative analysis program (GNAP) with examples of petrologic problem solving: U.S. Geological Survey Open-File Report 79–1237, 112 p.

Taggart, J. E., Jr., Lichte, F. E., and Wahlberg, J. S., 1981, Methods of analysis of samples using X-ray fluorescence and induction-coupled plasma spectroscopy, *in* Lipman, P. W., and Mullineaux, D. R., eds., The 1980 eruptions of Mount St. Helens, Washington: U.S. Geological Survey Professional Paper 1250, 844 p.

Thornton, C. P., and Tuttle, O. F., 1960, Differentiation index [Pt.] 1, *of* Chemistry of igneous rocks: American Journal of Science, v. 258, no. 9, p. 664–684.

Tuttle, O. F., and Bowen, N. L., 1958, Origin of granite in the light of experimental studies in the system $NaAlSi_3O_8$–$KAlSi_3O_8$–SiO_2–H_2O: Geological Society of America Memoir 74, 153 p.

Wright, T. L., 1968, X-ray and optical study of alkali feldspar—[Pt.] 2, An X-ray method for determining the composition and structural state from measurement of 2θ values for three reflections: American Mineralogist, v. 53, no. 1–2, p. 88–104.

Zielinski, R. A., Lipman, P. W., and Millard, H. T., Jr., 1977, Minor-element abundances in obsidian, perlite, and felsite of calc-alkalic rhyolites: American Mineralogist, v. 62, p. 426–437.

U S. GOVERNMENT PRINTING OFFICE: 1987—773-047/46,068 REGION NO 8